[22] E. B. Voura, J. K. Jaiswal, H. Mattoussi, and S. M. Simon, "Tracking metastatic tumor cell extravasation with quantum dot nanocrystals and fluorescence emission-scanning microscopy," *Nature Med.*, vol. 10, pp. 993–998, 2004.
[23] R. Hardman, "A toxicologic review of quantum dots: toxicity depends on physicochemical and environmental factors," *Environ. Health Perspect.*, vol. 114, pp. 165–172, 2006.
[24] A. Hoshino, K. Fujioka, T. Oku, M. Suga, Y. F. Sasaki, T. Ohta, M. Yasuhara, K. Suzuki, and K. Yamamoto, "Physicochemical properties and cellular toxicity of nanocrystal quantum dots depend on their surface modification," *Nano Lett.*, vol. 4, pp. 2163–2169, 2004.
[25] A. M. Derfus, W. C. W. Chan, and S. N. Bhatia, "Probing the cytotoxicity of semiconductor quantum dots," *Nano Lett.*, vol. 4, pp. 11–18, 2004.
[26] J. H. Warner, A. Hoshino, K. Yamamoto, and R. D. Tilley, "Water-soluble photoluminescent silicon quantum dots," *Angew. Chem. Int. Ed. Engl.*, vol. 44, pp. 4550–4554, 2005.

Satoru Yamamoto was born in Japan on August 30, 1964. He received the M.D. degree from the School of Medicine, Mie University, Japan, in 1992. He also studied at Wilmer Eye Institute, Johns Hopkins University, Baltimore, MD.

He is currently Director of the Department of Ophthalmology, Yokohama Sakae Kyousai Hospital, Yokohama, Japan. In university, he studied ophthalmology and especially skills in ophthalmic surgery. He is currently interested in quantum dots and their clinical applications in the field of ophthalmology.

Dr. Yamamoto is a member of the American Academy of Ophthalmology (AAO) and the Association for Research in Vision and Ophthalmology (ARVO), and a Fellow Researcher at the International Clinical Research Center, International Medical Center of Japan (IMCJ).

Noriyoshi Manabe photograph and biography not available at the time of publication.

Kouki Fujioka, photograph and biography not available at the time of publication.

Akiyoshi Hoshino, photograph and biography not available at the time of publication.

Kenji Yamamoto, photograph and biography not available at the time of publication.

American Journal of Physiology - Endocrinology and Metabolism

Am J Physiol Endocrinol Metab 289: E419–E428, 2005.
First published April 12, 2005; doi:10.1152/ajpendo.00512.2004.

Proteomic analysis on insulin signaling in human hematopoietic cells: identification of CLIC1 and SRp20 as novel downstream effectors of insulin

Kumiko Saeki,[1]* Etsuko Yasugi,[1]* Emiko Okuma,[1] Samuel N. Breit,[4] Megumi Nakamura,[3] Tosifusa Toda,[3] Yasushi Kaburagi,[2] and Akira Yuo[1]

[1]*Departments of Hematology and* [2]*Metabolic Disorder, Research Institute, International Medical Center of Japan;* [3]*Proteomics Collaboration Research Group, Tokyo Metropolitan Institute of Gerontology, Tokyo, Japan;* *and* [4]*Centre for Immunology, St. Vincent's Hospital, and University of New South Wales, Sydney, Australia*

Submitted 27 October 2004; accepted in final form 11 April 2005

Saeki, Kumiko, Etsuko Yasugi, Emiko Okuma, Samuel N. Breit, Megumi Nakamura, Tosifusa Toda, Yasushi Kaburagi, and Akira Yuo. Proteomic analysis on insulin signaling in human hematopoietic cells: identification of CLIC1 and SRp20 as novel downstream effectors of insulin. *Am J Physiol Endocrinol Metab* 289: E419–E428, 2005. First published April 12, 2005; doi:10.1152/ajpendo.00512.2004.—Insulin/IGF-I-dependent signals play important roles for the regulation of proliferation, differentiation, metabolism, and autophagy in various cells, including hematopoietic cells. Although the early protein kinase activation cascade has been intensively studied, the whole picture of intracellular signaling events has not yet been clarified. To identify novel downstream effectors of insulin-dependent signals in relatively early phases, we performed high-resolution two-dimensional electrophoresis (2-DE)-based proteomic analysis using human hematopoietic cells 1 h after insulin stimulation. We identified SRp20, a splicing factor, and CLIC1, an intracellular chloride ion channel, as novel downstream effectors besides previously reported effectors of Rho-guanine nucleotide dissociation inhibitor 2 and glutathione *S*-transferase-pi. Reduction in SRp20 was confirmed by one-dimensional Western blotting. Moreover, MG-132, a proteasome inhibitor, prevented this reduction. By contrast, upregulation of CLIC1 was not observed in one-dimensional Western blotting, unlike the 2-DE results. As hydrophilic proteins were predominantly recovered in 2-DE, the discrepancy between the 1-DE and 2-DE results may indicate a certain qualitative change of the protein. Indeed, the nuclear localization pattern of CLIC1 was remarkably changed by insulin stimulation. Thus insulin induces the proteasome-dependent degradation of SRp20 as well as the subnuclear relocalization of CLIC1.

HL-60 cells; PDQuest; matrix-assisted laser desorption ionization coupled to time-of-flight mass spectrometry; Mascot

INSULIN AND INSULIN-LIKE GROWTH FACTOR I (IGF-I) are known as important regulators of a variety of biological effects, including growth, development, and metabolism. Moreover, insulin-dependent signals contribute to the regulation of azurophil granule-selective macroautophagy in human hematopoietic cells (16). The molecular mechanisms for the actions of insulin and IGF-I have been intensively studied by various approaches, including gene-targeting animal experiments (1, 8, 14, 22) and molecular cloning techniques (20, 21). Now, the scenario for early intracellular signal transduction including a protein kinase activation cascade is well documented. It has been revealed that common intracellular signaling pathways are working downstream of insulin and IGF-I, including insulin receptor substrates (IRSs) (12) and Shc (17). The IRSs phosphorylate phosphatidylinositol 3-kinase to activate Akt, which transmits signals for proliferation and survival as well as the hematopoietic macroautophagy regulation (16), and the mammalian target of rapamycin and S6 kinase, which transmit signals for growth and translation besides heaptic macroautophagy regulation (2). On the other hand, Shc transmits signals for differentiation in hematopoietic cells (25).

In contrast to the early signal transduction, the picture of the later signaling events remains rather obscure. A large number of still undetermined molecules may be working downstream of the insulin-dependent signals. To obtain the whole picture of the intracellular signaling events downstream of the insulin receptor, comprehensive studies such as transcriptome analysis and proteome analysis may be especially powerful. A transcriptome analysis can illuminate the intracellular signaling events if they require new transcriptions or altered message stabilities. However, changes in protein expression are not always associated with those of the message expression, and vice versa. Thus transcriptome analysis would occasionally bring about false positive and/or false negative results. In this sense, proteome analysis is thought to be a more practical tool. Moreover, proteome analysis has merit in demonstrating protein modification changes such as phosphorylation and acetylation besides the change in net expression amounts. Indeed, studies on proteome analysis have successfully identified the protein molecules associated with metabolic regulation in the liver (3, 7). However, proteome analysis on insulin signaling in hematopoietic cells has not been performed despite the significance of insulin-dependent signals in the hematopoietic system.

For the first time, we performed proteomic analysis using human hematopoietic cells with the high-resolution two-dimensional electrophoresis (2-DE) system. We show that SRp20, a splicing factor, and CLIC1, an intracellular chloride ion channel, are working as novel downstream effectors of insulin signaling. The biological relevance of these events is discussed.

MATERIALS AND METHODS

Cells, growth factors, and inhibitors. HL-60 cells were maintained in RPMI 1640 medium (Life Technologies, Grand Island, NY) supplemented with 10% heat-inactivated fetal calf serum (FCS; JRH Bioscience, Lenexa, KS). For insulin-stimulating experiments, cells

* These authors contributed equally to this work. The order of the authors' names was arbitrarily arranged.

Address for reprint requests and other correspondence: A. Yuo, Dept. of Hematology, Research Institute, International Medical Center of Japan, 1-21-1 Toyama, Shinjuku-ku, Tokyo 162-8655, Japan (e-mail: yuoakira@ri.imcj.go.jp).

The costs of publication of this article were defrayed in part by the payment of page charges. The article must therefore be hereby marked "*advertisement*" in accordance with 18 U.S.C. Section 1734 solely to indicate this fact.

 0193-1849/05 $8.00 Copyright © 2005 the American Physiological Society

Downloaded from ajpendo.physiology.org on August 25, 2005

had been previously cultured in serum-free RPMI 1640 medium supplemented with 5 μg/ml human holo-transferrin (Sigma Chemical, St. Louis, MO) for 3 days, and then 5 μg/ml insulin (Sigma) were added. Transferrin was suspended in RPMI 1640 medium, and insulin was solubilized by 1 N hydrochloride. In some experiments, MG-132 (Calbiochem, La Jolla, CA) was added 30 min before insulin stimulation.

Two-dimensional gel electrophoresis with quantitative analyses. Insulin-depleted cells were stimulated by insulin. After a 1-h incubation, stimulated and nonstimulated cells were collected. After a washing with wash buffer (10 mM Tris·HCl buffer, pH 8.0, 5 mM magnesium acetate), 4×10^7 cells were suspended with 7 volumes of lysis buffer containing 2 M thiourea, 7 M urea, 4% (wt/vol) CHAPS, and 1 mM Pefabloc SC PLUS (Roche Diagnostics, Mannheim, Germany). The cell suspensions were kept for 10 min on ice, sonicated intermittently, and centrifuged at 12,000 *g* for 10 min at 4°C, and the supernatant fractions were collected. The protein concentration was determined in the lysis solution with a dye reagent from Amersham Biosciences (Piscataway, NJ), using BSA as a standard. The lysate was alkylated with Ready Prep Reduction-Alkylation Kit (Bio-Rad Laboratories, Hercules, CA). The 120 μg of protein lysate per gel were subjected to two-dimensional gel electrophoresis (2-DE). One-dimensional isoelectric focusing was carried out using Immobiline dry strip (18 cm long, pH 3–10 nonlinear or pH 4–7 linear, Amersham Biosciences) in a horizontal electrophoresis system (Ettan IPGphor, Amersham Biosciences) according to the manufacturer's instructions. After the one-dimensional elecrofocusing, IPG gels were equilibrated with buffer containing 50 mM Tris·HCl (pH 8.8), 6 M urea, 30% (vol/vol) glycerol, 2% (wt/vol) sodium dodecyl sulfate (SDS), 0.01% bromophenol blue, and 0.5% dithiothreitol, followed by alkylation with equilibration buffer containing 4.5% idoacetamide instead of 0.5% dithiothreitol at room temperature for 15 min. The gels were subjected to two-dimensional SDS-PAGE (10% gel). Proteins were visualized in the gels by staining with SYPRO Ruby Protein Gel Stain (Bio-Rad Laboratories) for overnight. The florescence intensity of each protein spot was digitally recorded by FluorImager 595 (Amersham Biosciences) using ImageQuaNT software and the differential protein expression quantitatively analyzed by PDQuest software (Bio-Rad Laboratories). The density of each spot was normalized by that of the smallest β-actin spot. Initially, all of the spots were roughly matched by an automatic program in PDQuest software, which was followed by a more detailed manual matching process to correct inappropriate matching pairs. Three to six independent experiments were performed, and the results were statistically analyzed by Student's *t*-test.

Mass spectrometric analysis. Mass spectrometric analysis was performed according to the method reported by Toda et al. (23), with slight modifications. Briefly, each protein spot in SYPRO Ruby-stained gels was picked by FluoroPhoreStar 3000 (Anatech, Tokyo, Japan). The pieces of gels were dehydrated in 50% acetonitrile and 50% ammonium bicarbonate, next in 100% acetonitrile, and dried. The proteins were digested with 5 μg/ml trypsin (sequencing grade modified trypsin; Promega, Madison, WI) at 30°C. After overnight protein digestion, peptide fragments in the digest were subjected to matrix-assisted laser desorption ionization (MALDI) coupled to a time-of-flight (TOF) (MALDI-TOF) mass spectrometer (AXIMA-CFR; Shimazdu, Kyoto, Japan) for peptide mass fingerprinting (PMF). Protein identification was performed with the Mascot server (Matrix Science, Boston, MA) and Protein Prospector (UCSF Mass Spectrometry Facility, San Francisco, CA). We selected the *Homo sapiens* database of SWISS-PROT and parameters: peptide tolerance ± 0.4 Da and one missed cleavage. Carbamidomethyl modification of cysteine and acetylation of the NH_2-terminal end or lysine and phosphorylation of serine, threonine, or tyrosine were considered. Protein identification was repeated at least once with spots from different gels. Phosphorylated peptides were confirmed by MALDI-TOF-MS in a postsource decay (PSD) mode of AXIMA-CFR and AXIMA-CFRplus (Shimadzu). NH_2-terminal acetylation was determined by MALDI-QIT-TOF-MS in an MS/MS mode (AXIMA-QIT, Shimadzu).

One-dimensional Western blotting. Cells (5×10^5) were lysed with 100 μl of 1× Laemmli's sample buffer and boiled. Ten microliters of this lysate were subjected to SDS-PAGE with 15% gels. The electric transfer onto a polyvinylidene difluoride (PVDF) membrane was carried out with a semidry blotting apparatus (Bio-Rad Laboratories) at 50 mA/cm^2 for 45 min at room temperature using buffer containing 2.25% Tris, 10.8% glycine, and 20% methanol. The first antibody reaction was performed using anti-SRp20 antibody (7B4; Santa Cruz Biotechnology, Santa Cruz, CA), anti-Rho-guanine nucleotide dissociation inhibitor (Rho-GDI) antibody (A-20; Santa Cruz Biotechnology), anti-β-tubulin antibody (H-235; Santa Cruz Biotechnology), a sheep anti-CLIC1 antiserum (25), anti-cyclin D3 antibody (C-16; Santa Cruz Biotechnology), anti-cyclin E antibody (M-20; Santa Cruz Biotechnology), and anti-cyclin A antibody (BF683; Upstate Biotechnology, Lake Placid, NY). The second antibody reaction and the final detection procedure were performed using ECL Western blotting detection reagents (Amersham Biosciences) or SuperSignal West Dura Extended Duration Substrate (Pierce Biotechnology, Rockford, IL) according to the manufacturers' guidance. Information of the chemical luminescence was analogically developed onto Hyperfilm (Amersham Biosciences). After scanning of the developed film, the band intensities were calculated by ImageQuant software (Amersham Biosciences). Stripping of the first antibody was performed by incubating the PVDF membrane with Restore Western Blot Stripping Buffer (Pierce Biotechnology) at room temperature for 30 min.

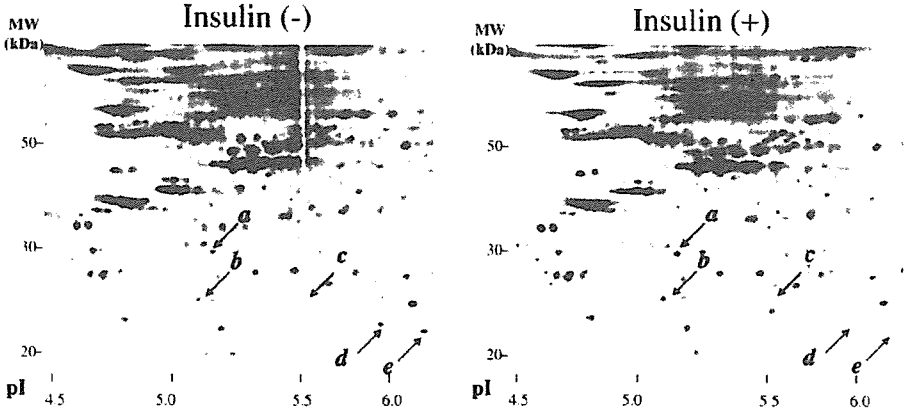

Fig. 1. Two-dimensional electrophoresis (2-DE) profile of human hematopoietic HL-60 cells with or without insulin treatment. HL-60 cells were cultured with transferrin-supplemented serum-free medium for 3 days. Then buffer solution (*left*) or 5 μg/ml insulin (*right*) was added, and cells were cultured for another 1 h at 37°C. Cell lysates were prepared as described in Experimental Procedures, and 2-DE was carried out. PDQuest software-based analysis demonstrated that the 5 spots (indicated by arrows) showed significant differences in their expressions with or without insulin treatment. *Spot a*, CLIC1, an intracellular chloride ion channel; *spot b*, Rho-guanine nucleotide dissociation inhibitor 2 (Rho-GDI-1); *spot c*, and glutathione *S*-transferase-pi (GST-pi); *spots d* and *e*, SRp-20, a splicing factor; *isoform of β-actin.

American Journal of Physiology – Endocrinology and Metabolism

Downloaded from ajpendo.physiology.org on August 25, 2005

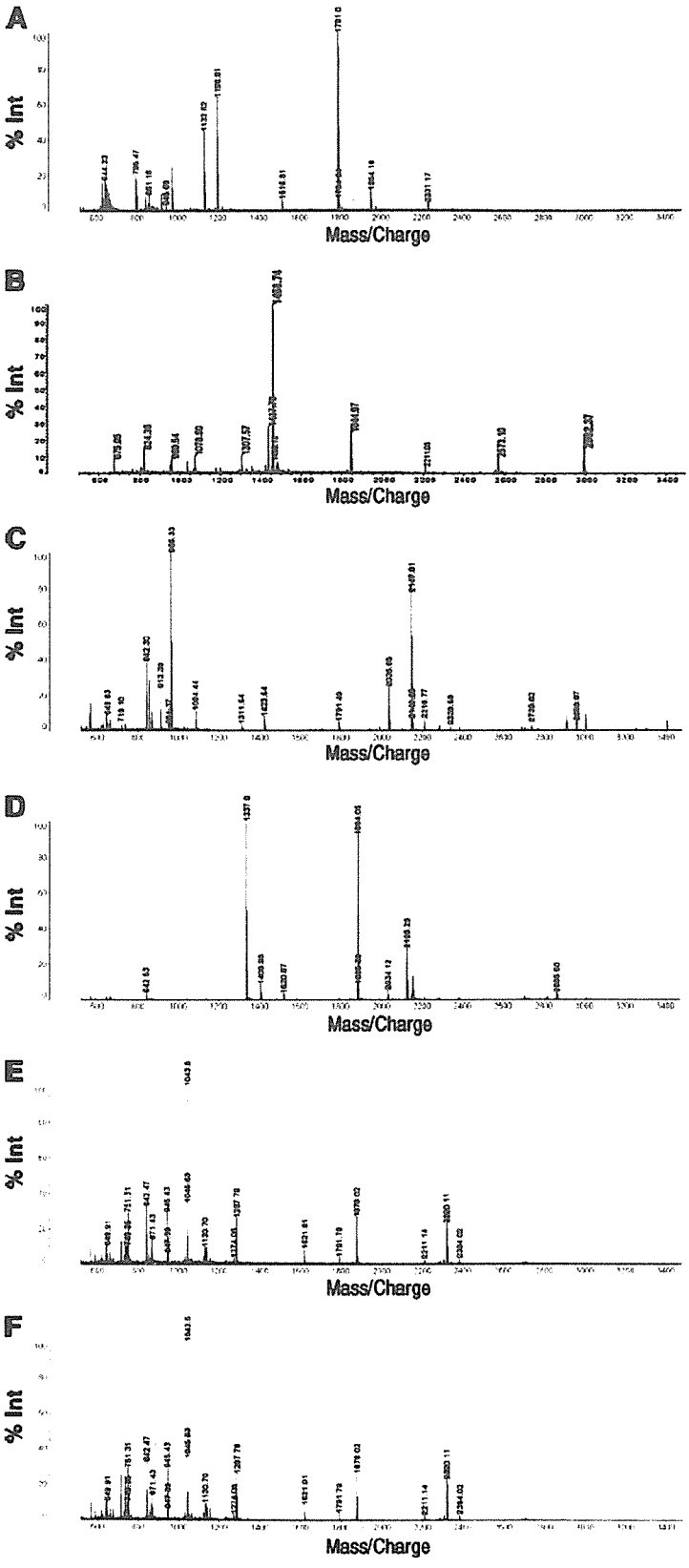

Fig. 2. Peptide mass fingerprinting (PMF) of *spots a–e*. *Spots a* (*B*), *b* (*C*), *c* (*D*), *d* (*E*), *e* (*F*) were picked, and, after trypsin digestion, matrix-assisted laser desorption ionization coupled to a time-of-flight mass spectrometer (MALDI-TOF-MS) analysis was performed. As a positive control, a β-actin spot (* in Fig. 1) was picked and analyzed (*A*).

American Journal of Physiology – Endocrinology and Metabolism

Downloaded from ajpendo.physiology.org on August 25, 2005

Two-dimensional Western blotting. SYPRO Ruby-stained proteins on gels were resolubilized and transferred according to our previously reported method (23). Briefly, the stained gel was incubated in resolubilization buffer (0.2% wt/vol SDS, 0.3% wt/vol Tris, 0.7% wt/vol glycine) for 10 min and mounted onto a PVDF membrane in a semidry blotting apparatus (Bio-Rad Laboratories). Electrotransfer was carried out at 4 V/cm^2 for 1 h at room temperature using buffer containing 0.3% (wt/vol) Tris, 1.5% (wt/vol) glycine, 0.1% (wt/vol) SDS. The florescence images of the blotted PVDF membranes were scanned and recorded by FluorImager 595 (Amersham Biosciences). The PVDF membranes were further subjected to immunoblotting as in cases of 1-DE Western blotting.

Cell cycle analysis. Cells (5×10^5) were collected, washed with PBS, and fixed with 70% ice-cold ethanol for 4 h. After treatment with RNase A (100 μg/ml, Sigma) for 30 min at 37°C, DNA was stained with 50 μg/ml propidium iodide (Sigma). Cell cycle analysis was performed by FACScalibur (Becton-Dickinson, Mountain View, CA) using CELL Quest software according to the manufacturer's guidance.

Immunocytochemistry. Cells were fixed on slide glasses with a cytospin apparatus (Cytospin2; Shandon, Pittsburgh, PA) with further fixation with acetone-methanol solution (1:3). The immunostaining procedure was performed as described elsewhere (16) using anti-CLIC1 antibody (1:1,000 dilution) (24). The cells were observed by fluorescent microscopy with Normarsky differentiated interference contrast (Olympus Optical, Tokyo, Japan).

Statistical analysis. Student's *t*-test was used to determine statistical significance. A P value of <0.05 was considered significant.

RESULTS

2-DE protein expression profiles of human hematopoietic cells with or without insulin treatment. To identify novel downstream effectors in early phases of insulin-dependent signals in human hematopoietic cells, we performed the 2-DE-based differential protein expression analysis using human myeloblastic HL-60 cells. The cells which had been cultured in the absence of insulin for 3 days were treated with 5 μg/ml insulin or water. After 1 h, cell lysates were prepared according to the standard isoelectric focusing electrophoresis method described in MATERIALS AND METHODS. In this procedure, highly hydrophobic, urea-insoluble proteins were eliminated during the centrifugation step as precipitants, and only the supernatant fractions were used for 2-DE. In preliminary experiments, we used the immobilized pH gradient gel strip with a broad pH range (pH 3–10 nonlinear) for one-dimensional isoelectric focusing. Although more than 1,000 protein spots were visualized after SYPRO Ruby staining, PDQuest software-based analysis indicated that the spots having significant expression changes by insulin treatment were mainly located at pH 4–6 in the horizontal axis (data not shown). Thus we performed the following detailed analysis using the immobilized pH gradient gel strip with a narrower range (pH 4–7 linear) for finer resolution (Fig. 1). Over 600 protein spots were visualized by SYPRO Ruby staining. From these spots, we selected the candidates for the subsequent mass spectrometric analysis according to the following criteria. The basal expression level was higher than 5% of that of the largest β-actin spot, and the increase or decrease in the expression after insulin stimulation was greater than twofold or less than one-half, respectively. After statistical analysis of the multiple experiments (n = 3–6), five candidates were determined (Fig. 1). These spots were picked from the gel and, after trypsin digestions, MALDI-TOF-MS analysis was performed. Figure 2 shows the PMF of each spot, with a PMF of β-actin as a positive control. These data were further analyzed, being sent to the Mascot search server, and it was suggested that *spot a* was CLIC1, *spot b* was Rho-GDI-2, *spot c* was glutathione *S*-transferase-pi (GST-pi), and *spots d* and *e* were SRp20 (Fig. 2 and Table 1). The Mascot score of each search result was 175 (*spot a*), 80 (*spot b*), 98 (*spot c*), 100 (*spot d*), and 64 (*spot e*), indicating that the protein identifications by PMF were highly reliable (the data are summarized in Table 1). The results of the statistical analysis for the expression amounts of these spots are summarized in Table 2. Among these spots, Rho-GDI-2 (*spot b*) and GST-pi (*spot c*) have already been identified as downstream effectors of insulin. Rho-GDI-2 is reportedly released from the intracellular membrane fractions to the cytoplasm by insulin (19), and the expression of GST-pi markedly increases after insulin stimulation (6). Thus we focused our research on the evaluation of *spot a* and *spots d* and *e*.

To confirm the Mascot search results, we performed 2-DE western blotting by transferring SYPRO Ruby-stained 2-DE protein spots to PVDF membrane. As shown in Fig. 3*A*, most of the proteins were properly transferred to the membrane with a SYPRO Ruby pattern similar to that of the original gel. As shown in Fig. 3*B*, *spot a* was indeed recognized by anti-CLIC1

Table 2. *Ratios of spot intensities (insulin +/insulin −)*

Spot	Protein	Means ± SD	*P* Value
a	CLIC1	1.83 ± 0.37	<0.01
b	Rho-GDI-2	2.03 ± 0.43	<0.02
c	GST-pi	1.93 ± 0.52	<0.05
d	SRp20	0.24 ± 0.33	<0.01
e	SRp20	0.18 ± 0.27	<0.005

Summarized results from 3–6 independent experiments are shown. Statistical analysis was performed by Student's *t*-test.

Table 1. *Protein identification by mass spectrometry analysis*

Spot	GenBank Acc. No.	Protein Name	Mr		pI		Mascot Score	Peptides		Sequence Coverage, %
			Theo, Da	Obs, kDa	Theo	Obs		Match	Total	
a	O00299	CLIC1	2.7248	29.0	5.09	5.16	175	10	11	47
b	P52566	Rho-GDI-2	2.3031	23.6	5.10	5.08	80	6	9	24
c	P09211	GST-pi	2.3438	22.9	5.44	5.67	98	6	8	48
d	P23152	SRp20	1.9546	21.2	11.64	6.13	100	9	11	43
e	P23152	SRp20	1.9546	20.5	11.64	6.38	100	9	11	43

Values of theoretical isoelectric points (pI) and molecular weights/masses (Mr) were obtained from Mascot search results. Theo, theoretical; Obs, observed; CLIC1, intracellular chloride ion channel; Rho-GDI-2, Rho-guanine nucleotide dissociation inhibitor 2; GST-pi, glutathione-*S*-transferase-pi; SRp20, a splicing factor. Calculations of experimental isoelectric point (pI) and molecular weight (Mr) were based on migration of the protein spot on 2-D gels using PDQuest.

American Journal of Physiology – Endocrinology and Metabolism

Downloaded from ajpendo.physiology.org on August 25, 2005

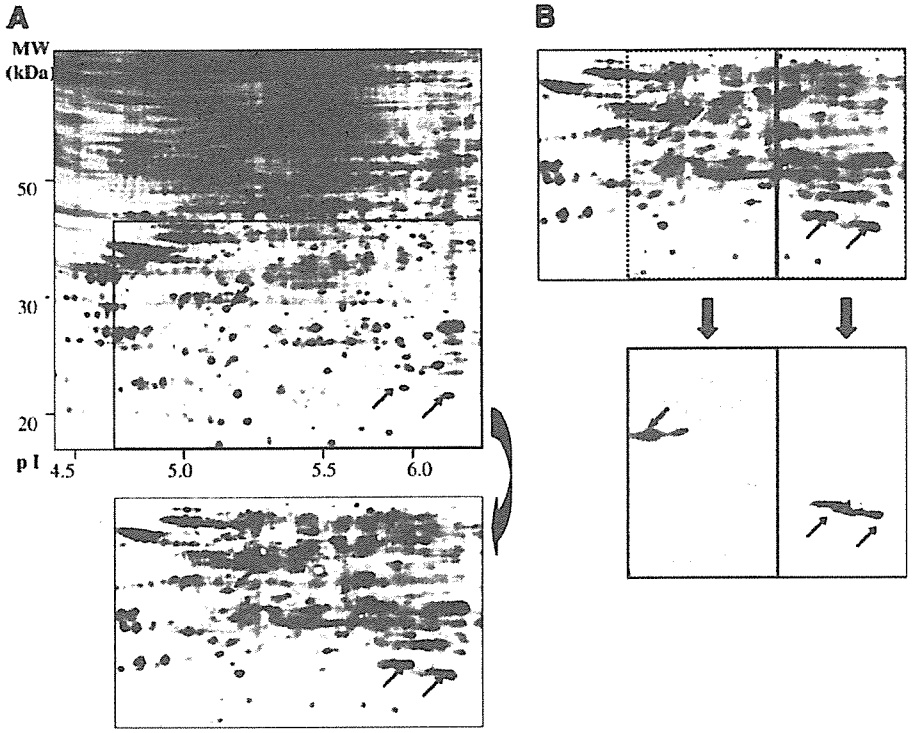

Fig. 3. 2-DE Western blotting. *A*: SYPRO Ruby-stained 2-DE gel, in which the lysate of buffer solution-treated cells were applied as in Fig. 1, *left*, was trimmed (*top*) and transferred onto a PVDF membrane (*bottom*). Transferred proteins were visualized by fluorescence image scanner. *B*: PVDF membrane was cut as indicated and blotted by anti-CLIC1 antiserum (*bottom left*) or anti-SRp20 antiserum (*bottom right*). Spots for CLIC1 and SRp20 are indicated with black arrows. Note that there is an extra spot on the anti-CLIC1-blotted membrane (indicated with white arrow).

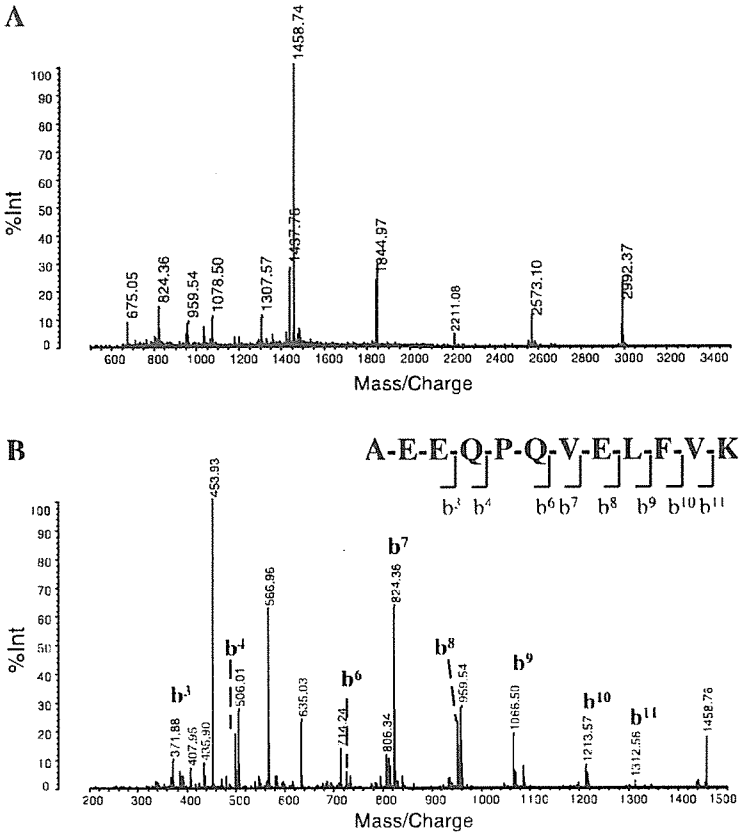

Fig. 4. Amino acid sequencing of NH_2-terminal peptide fragment of CLIC1. Parent ion at *m/z* 1,458.74 in Fig. 2*B* in insulin-treated cells was subjected to subsequent analysis using MS/MS mode of MALDI-TOF-MS (AXIMA-QIT). The mass data of b-series of the product ions were analyzed by the PepSeq program in ProteinLynx software. NH_2-terminal acetylated peptides of *N*-acetyl-AEE (*m/z* 372.14, b^3 ion), *N*-acetyl-AEEQ (*m/z* 500.20, b^4 ion), *N*-acetyl-AEEQPQ (*m/z* 725.30, b^6 ion), *N*-acetyl-AEEQPQV (*m/z* 824.38, b^7 ion), *N*-acetyl-AEEQPQVE (*m/z* 953.42, b^8 ion), *N*-acetyl-AEEQPQVEL (*m/z* 1,066.50, b^9 ion), *N*-acetyl-AEEQPQVELF (*m/z* 1,213.57, b^{10} ion), and *N*-acetyl-AEEQPQVELFV (*m/z* 1,312.64, b^{11} ion) were detected. Peptide mass fingerprinting (PMF; *A*) and MS/MS data of b-series (*B*) are shown. Similar analysis concerning control cells also demonstrated NH_2-terminal acetylation of CLIC1 (data not shown).

American Journal of Physiology – Endocrinology and Metabolism

Downloaded from ajpendo.physiology.org on August 25, 2005

antibody and *spots d* and *e* were recognized by anti-SRp20 antibody. We also studied the possible modifications on these two proteins. As shown in Fig. 1*A*, the observed isoelectric point (pI) of CLIC1 was 5.16, which is similar to the Mascot information (the calculated pI was 5.09). Interestingly, there was an extra small spot with a higher pI value (Fig. 3*B*, white arrow). Indeed, we detected a doublet band in one-dimensional Western blotting, where the lysate prepared for 2-DE was mixed with an isovolume of 2× Laemmli's sample buffer and subjected to SDS-PAGE (data not shown and see Fig. 6*B*). Thus CLIC1 is expressed in at least two forms with different pI values in human hematopoietic cells, although the molecular basis for this difference was not elucidated. The MS digest analysis of *spot a* in the 2-DE profiles of both the insulin-treated and control cells demonstrated that the peptide fragment at mass-to-charge ratio (*m/z*) 1,458.74 in PMF of *spot a* represented the NH_2 terminus acetylated fragment acetyl-AEEQPQVELFVK, indicating that the first methionine was eliminated and the second alanine was N-acetylated. This finding was indeed confirmed by the amino acid sequencing at the *m/z* 1,458.74 fragment by the MS/MS mode of MALDI-TOF-MS, as shown in Fig. 4.

As for SRp20, the observed pI values of *spots d* and *e* were 6.13 and 6.38, respectively (Fig. 1 and Table 1), in contrast to the Mascot software information (the calculated pI was 11.64). This discrepancy may come from the modifications of SRp20. The MS digest analysis indicated that the SRp20 was phosphorylated at two sites, including Ser^{115} and Ser^{108}, from the existence of the peptide fragment ions of *m/z* 751.31 and *m/z* 945.43 (Fig. 5*A*). Mass value of *m/z* 751.31 is speculated amino acid sequences as $RRSPR_{(113-117)}$, $RSPRR_{(114-118)}$, or $SPRRR_{(115-119)}$ (Fig. 5*E*). As concerns *m/z* 945.43, MS digest suggests the amino acid sequence as $RRSPPPR_{(106-112)}$, $RSPPPRR_{(107-113)}$, or $SPPPRRR_{(108-114)}$. Phosphorylated peptide was confirmed by MALDI-TOF-MS in a seamless PSD mode (AXIMA-CFR) that detected the neutral loss of phosphate group. As shown in Fig. 5, *B* and *C*, phosphorylation-dependent neutral loss (−80 Da) and dehydration (−18 Da) were detected in the fragments at *m/z* 751.31 and *m/z* 945.43. Conversely, the MALDI-TOF-MS PSD spectrum of the control peptide ion gated at *m/z* 1,043.57 showed no significant neutral loss (Fig. 5*D*). Next, the amino acid sequences of *m/z* 751.31, *m/z* 945.43, and *m/z* 1,043.57 were examined by the same method as described above by using AXIMA-CFRplus. The amino acid sequences of *m/z* 751.31 could not be determined because the fragment ion was low intensity (data not shown). However, it is presumable that the Ser^{115} is phosphorylated. From the mass spectra of gated ion at *m/z* 945.43, the amino acid sequence was determined as $RRSPPPR_{(106-112)}$, and the position of phosphorylation was Ser^{108} (Fig. 6*A*). As a

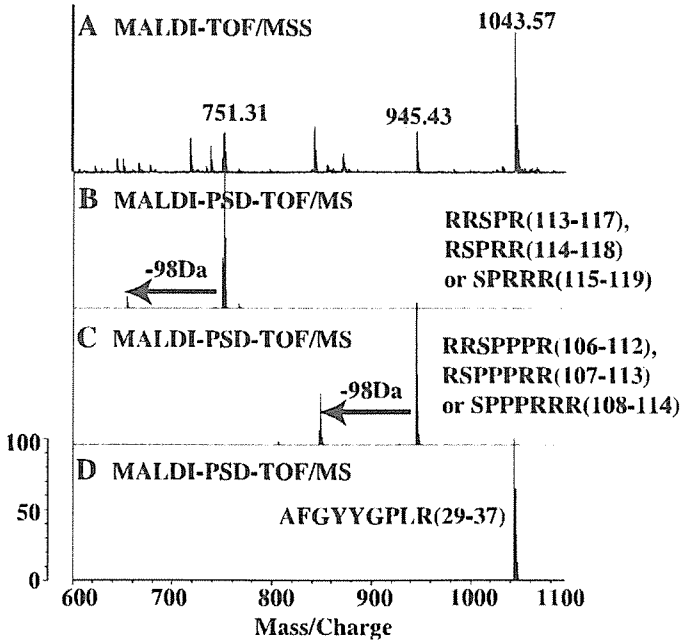

E 1 MHRDSCPLDC KVYVGNLGNN GNKTELERAF GYYGPLRSVW VARNPPGFAF

m/z 1043.57

51 VEFEDPRDAA DAVRELDGRT LCGCRVRVEL SNGEKRSRNR GPPPSWGRRP

101 RDDYRRRSPP PRRRSPRRRS FSRSRSRSLS RDRRRERSLS RERNHKPSRS

m/z 945.43 *m/z* 751.31

151 FSRSRSRSRS NERK

Fig. 5. Confirmation of SRp20 phosphorylation at specific serine residues. *A*: gated ions at *m/z* 751.31, 945.43, and 1,043.57 in Fig. 2*E* were subjected to analysis of neutral loss by MALDI-TOF-MS (AXIMA-CFR) in post-source decay (PSD) mode. The 98-Da loss of mass values was detected in gated ion at *m/z* 751.31 (*B*) and *m/z* 945.43 (*C*), but not in gated ion at *m/z* 1,043.57 (*D*) as a negative control. *E*: primary sequence of SRp20. *Phosphorylated amino acid.

American Journal of Physiology – Endocrinology and Metabolism

Downloaded from ajpendo.physiology.org on August 25, 2005

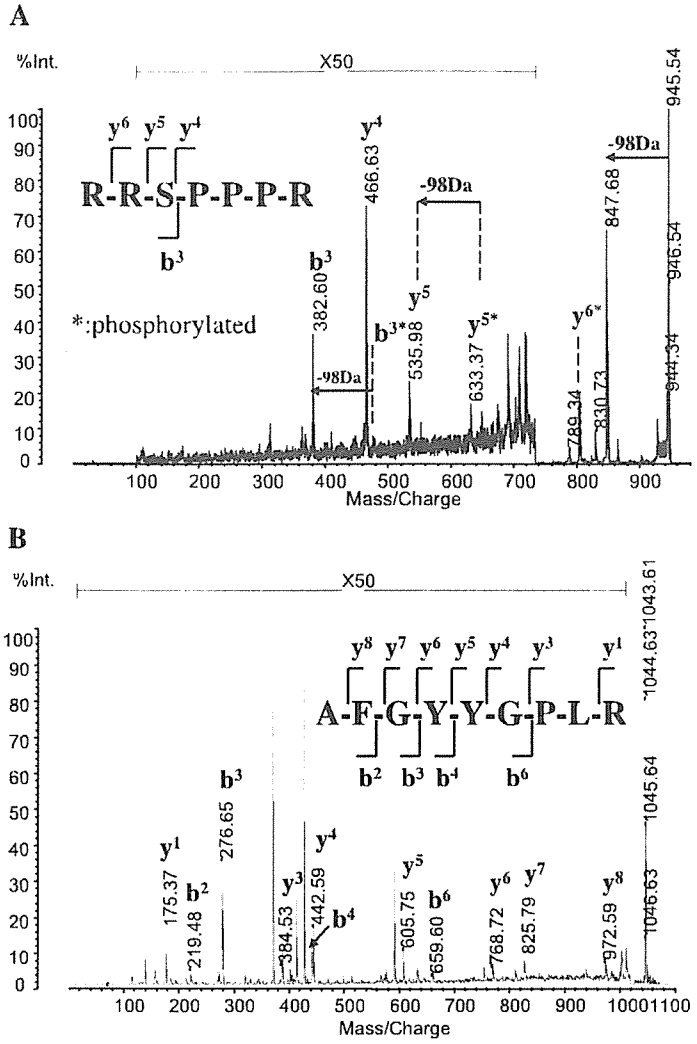

Fig. 6. Sequence analysis of gated ions at *m/z* 945.43 and 1,043.57 by MALDI-TOF-MS in PSD mode. *A*: gated ion at *m/z* 945.29 in Fig. 5*C* was subjected to subsequent analysis using PSD mode of MALDI-TOF-MS (AXIMA-CFRplus) *B*: three neutral loss ions (−98 Da) of *m/z* 480, 633, and 945 were detected. Gated ion at *m/z* 1,043.57 in Fig. 5*D* was subjected to the same analysis. Neutral loss ion (−98 Da) was not detected.

negative control, *m/z* 1,043.57 was subjected to analysis using PSD mode of AXIMA-CFRplus (Fig. 6*B*). The amino acid sequence was decided as AFGYYGPLR$_{(29\ 37)}$, which was not phosphorylated. These results indicated that Ser^{115} and Ser^{108} were phosphorylated in human hematopoietic cells (Fig. 5*E*). Thus the two phosphorylations of SRp20 may be responsible for the acidic shift of SRp20 in 2-DE.

Thus the 2-DE-based differential protein expression analysis identified CLIC1 and SRp20 as novel downstream effectors of insulin in human myeloblastic HL-60 cells.

1-DE study of CLIC1 and SRp20 expressions after insulin stimulations. It is known that there are occasionally discrepancies between the results of 2-DE and 1-DE. The difference in the protein solubilization capacities between the two systems is thought to be one of the reasons. During cell lysate preparation in 2-DE, highly hydrophobic proteins are prone to make precipitations and thus be eliminated from the lysates after centrifugation. Thus the protein expression changes in 2-DE-based proteome analysis not only means that the net protein expression changes but also the changes in protein solubilization. So we studied the expressions of CLIC1 and SRp20 after insulin stimulation by 1-DE Western blotting.

In contrast to the results of 2-DE, there was no significant difference in CLIC1 expression between insulin-treated and nontreated samples in 1-DE (Fig. 7*A*). Moreover, CLIC1 was detected as a single band, unlike the 2-DE results, where CLIC1 was detected as two spots. Interestingly, CLIC1 was detected as a doublet band, and the expression amounts of CLIC1 were indeed upregulated by insulin stimulation when the 2-DE lysates were treated by an isovolume of 2× Laemmli's buffer and subjected to 1-DE (Fig. 7*B*, *lane 2*). These findings strongly suggest that insulin treatment induced certain qualitative changes of CLICL1. Compared with 1-DE, the protein recovery rate in 2-DE was generally low: one-fourth the recovery as for CLIC1 (Fig. 7*B*, compare *lanes 1* and *3*) and one-eighth the recovery as for β-tubulin (Fig. 7*B*, compare *lanes 1* and *3*). However, the expression amounts of β-tubulin (Fig. 7*B*, compare *lanes 1* and *2*) and α-tubulin (data not shown) were not significantly changed by insulin treatment even in 2-DE lysates. By contrast, around a twofold increment in CLIC1 was reproducibly observed after insulin stimulation (Fig. 7, *B* and *C*, and data not shown). We then examined the possibility that the insulin-mediated increments in CLIC1 in 2-DE lysate were associated with the changes in its subcellular

American Journal of Physiology – Endocrinology and Metabolism

Downloaded from ajpendo.physiology.org on August 25, 2005

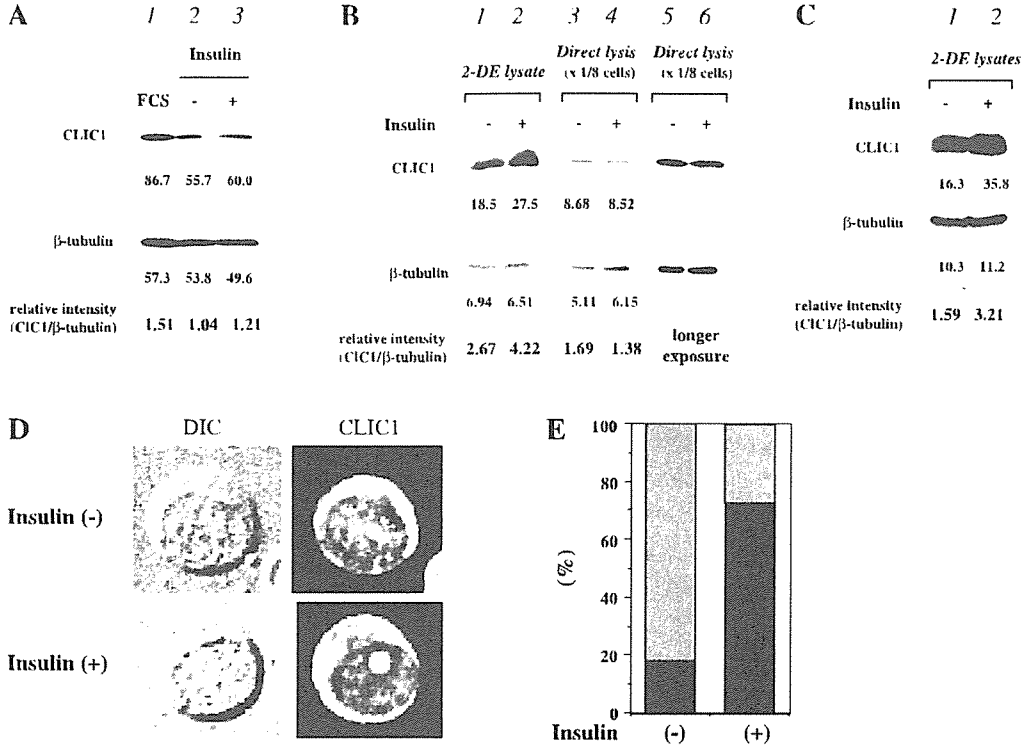

Fig. 7. 1-DE Western blotting of CLIC1. Cells that had been cultured with transferrin-supplemented serum-free medium for 3 days were stimulated by buffer solution (*lane 2*) or insulin (*lane 3*) and incubated for another 1 h at 37°C. *A*: cells were directly lysed with 1× Laemmli's sample buffer and subjected to 1-DE. Western blotting was performed using anti-CLIC1 antiserum. The lysate of the cells that had been cultured in the presence of FCS was also subjected to 1-DE (*lane 1*). Numeral under each band indicates intensity of the protein band. After the first antibody was stripped, the PVDF membrane was reblotted with anti-β-tubulin antibody. *B*: cell lysates prepared according to 2-DE protocol were mixed with isovolume of 2× Laemmli's sample buffer (*lanes 1* and *2*). One-eighth of the cells were directly lysed with 1× Laemmli's sample buffer and subjected to 1-DE (*lanes 3* and *4*). Longer exposure results of *lanes 3* and *4* are shown in *lanes 5* and *6*, respectively. *C*: results of independently performed experiment from *B* are shown. *D* and *E*: subcellular localization of CLIC1. *D*: insulin-treated or nontreated HL-60 cells were stained with anti-CLIC1 antibody. DIC, photograph with Normarsky differentiated interference contrast. *E*: percentages of cells with nuclear speckled staining pattern (filled bars) and cells with nucleoli-staining pattern (gray bars) are shown.

localization. As shown in Fig. 7, *D* and *E*, the nuclear localization pattern of CLIC1 was clearly changed by insulin treatment: CLIC1 was detected mainly as speckled forms in nuclear matrix in nontreated cells, whereas CLIC1 was located mainly at nucleoli in insulin-treated cells. Thus the changes in subnuclear localization may responsible for the expressional changes of CLIC1 in 2-DE.

Next, we studied the expression of SRp20 in 1-DE Western blotting. The SRp20 expression was actually reduced as in the case of 2-DE (Fig. 8*A*), indicating that the total amount of SRp20 was reduced by insulin treatment. To further investigate the molecular basis of insulin-mediated reduction in SRp20, the effects of the proteasome inhibitor MG-132 were examined. As shown in Fig. 8*B*, MG-132 inhibited the insulin-mediated reduction of SRp20 in a dose-dependent manner. MG-132 also blocked the degradation of cyclin D3 and enhanced the accumulation of cyclin D3 after insulin stimulation (Fig. 8*B*, *lane 5*). Interestingly, the recovery of SRp20 expres-

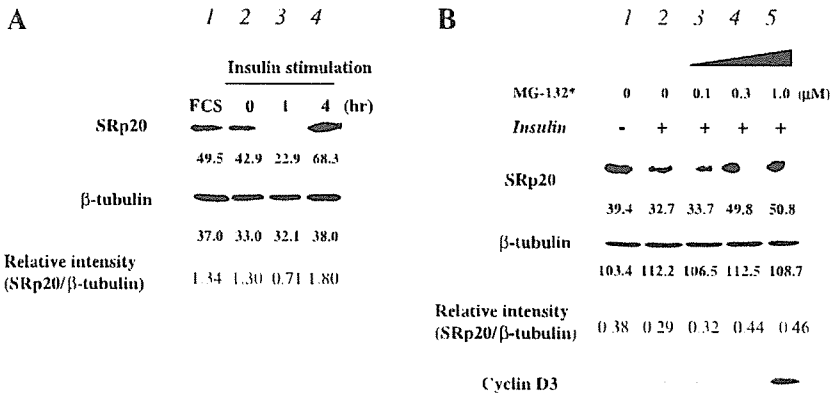

Fig. 8. 1-DE Western blotting of SRp20. Cells were cultured with transferrin-supplemented serum-free medium for 3 days. *A*: cells were then stimulated with insulin, and cell lysates were prepared at indicated times (*lanes 2–4*). Western blotting was performed using anti-SRp20 antiserum. The lysate of cells cultured in the presence of FCS was also subjected to 1-DE (*lane 1*). Numeral under each band indicates intensity of protein band. After the first antibody was stripped. PVDF membrane was reblotted with anti-β-tubulin antibody. *B*: DMSO or increasing doses of MG-132 were added 30 min before insulin stimulation. Cell lysates were prepared 1 h after stimulation and subjected to 1-DE. Western blotting was performed using anti-SRp20 antiserum. PVDF membrane was reblotted with anti-β-tubulin antibody and further with cyclin D3 antibody.

American Journal of Physiology – Endocrinology and Metabolism

Downloaded from ajpendo.physiology.org on August 25, 2005

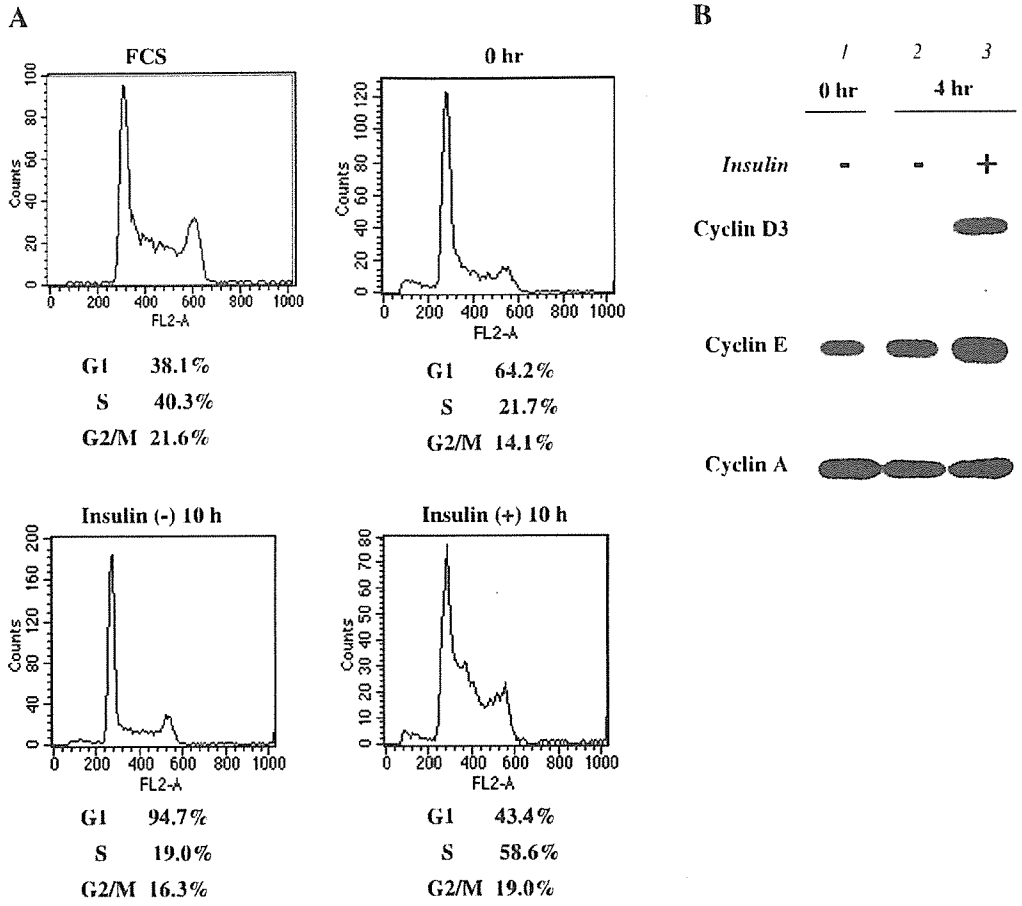

Fig. 9. Cell cycle analysis and expressions of cyclins. *A*: cells cultured with transferrin-supplemented serum-free medium for 3 days were stimulated with buffer solution (*bottom left*) or insulin (*bottom right*). After another 10-h incubation at 37°C, cells were fixed with 70% ethanol and subjected to DNA content assessment by fluorescence-activated cell sorting. Cells cultured in the presence of serum were also subjected to flow cytometric analysis (*top left*). *B*: cells cultured with transferrin-supplemented serum-free medium for 3 days were stimulated with buffer solution (*lane 2*) or insulin (*lane 3*). Cell lysates were prepared after another 4-h incubation. Western blotting was performed using anti-cyclin D3, followed by anti-cyclin E and anti-cyclin A reblotting.

sion was observed 4 h after stimulation (Fig. 8*A*, *lane 4*). Because serum stimulation activates SRp20 transcription and increases the protein expression of SRp20 as the cells enter into S-phase (9), the recovery in SRp2 expression would be associated with the cell cycling progression. As shown in Fig. 9, the insulin treatment significantly increased the S-phased population. Thus the recovery in SRp20 in later phases is associated with an enhanced S-entry.

Thus insulin treatment causes qualitative changes of CLIC1 that are associated with its subnuclear localization and the proteasome-dependent degradations of SRp20 as early as 1 h.

DISCUSSION

We identified CLIC1 and SRp20 as novel downstream effectors of insulin-dependent signals in human hematopoietic cells by using a 2-DE-based proteome analytic system.

A 2-DE-based proteome analysis has merit in managing a wide spectrum of protein expressions atone time. Moreover, it can illustrate the change in modifications and subcellular localization of the proteins besides the change in net amounts. As in the case of CLIC1, glyceraldehyde-3-phosphate dehydrogenase (GAPDH) expressions in 2-DE were upregulated by insulin stimulation, although no significant changes were detected in 1-DE (K. Saeki, unpublished observation). Because serum stimulation, which often induces similar protein expression changes as insulin stimulation, reportedly induces cytoplasmic transport of GAPDH (18), the upregulated expression of GAPDH in 2-DE may be associated with similar subcellular translocation.

Although CLIC1 functions as a chloride ion channel when localized to membranes (26), it is known that CLIC1 localizes principally to the cell nucleus in human hematopoietic cells (24). CLIC1 is structurally homologous to the GST superfamily of proteins with a redox-active site at the NH_2 terminus (5). It is suggested that CLICL1 activity is under the control of redox-active signaling molecules in vivo (5). In this sense, it is interesting that GST-pi is also a downstream effector of insulin as we showed (Fig. 1*A*, *spot c*) and reported elsewhere (6). It is known that hyperglycemia and, to a lesser extent, insulin resistance cause oxidative stress (15, 13). Insulin signaling might possibly contribute to the reduction of oxidative stresses by changing the expression patterns of CLICL1 and GST-pi. Further investigations are required to understand the molecular basis and biological relevance of insulin-induced changes in CLIC1 in the 2-DE system.

American Journal of Physiology – Endocrinology and Metabolism

Downloaded from ajpendo.physiology.org on August 25, 2005

As for *spots d* and *e* of SRp20, we could not find any differences in PMFs. One interpretation is that distinct phosphorylations took place at their COOH-terminal SR domains. Because the SR domain is extremely rich in arginine residues, this domain should be degraded into pieces after trypsin digestion, and, as a result, the peptide fragment ions might be hardly detectable. In any case, the expressions of *spots d* and *e* were both decreased by insulin stimulation, and thus the precise determination of structural differences between the two spots would be a less important subject for an understanding of biological effects of insulin. As we showed, the insulin-induced reduction in SRp20 was inhibited by pretreatment of the cells by MG-132, a reversible proteasome inhibitor (Fig. 8*B*). Quite unexpectedly, lactacystin, an irreversible proteasome inhibitor, could not inhibit the reduction of SRp20, although it effectively enhanced an insulin-dependent accumulation of cyclin D3 (K. Saeki, unpublished observation), suggesting that there might be at least two different proteasome-dependent protein degradation systems with distinct lactacystin susceptibilities.

What is the impact of SRp20 reduction by insulin? SRp20 is a splicing factor involved in the regulation of alternative splicing of certain precursor RNA, including SRp20 itself. Its roles for embryogenesis have been shown: an inactivation of SRp20 gene in mice resulted in a failure to form blastocysts, and embryos died at morula stage (11). Although complete loss of SRp20 functions is toxic, its mild reduction may play roles in particular situations. It is reported that overexpression of ASF/SF2, an alternative splicing regulator that antagonizes the function of SRp20 (10), was detected in malignant ovarian tissues (4). A transient reduction of SRp20 by insulin might upregulate the activity of ASF/SF2 and thus trigger signals for cell proliferation. Further investigations are required to determine the in vivo significance of a transient reduction of SRp20 after insulin stimulation.

ACKNOWLEDGMENTS

We greatly thank Masaki Yamada and Tsutomu Nishine of Shimadzu Corporation for technical assistance with the amino acid sequence analysis performed using an MS/MS and PSD mode of MALDI-TOF-MS (AXIMA-QIT and AXIMA-CFRplus).

GRANTS

This work was supported, in part, by a grant for diabetes research (MF-4) from the Organization for Pharmaceutical Safety and Research (to Y. Kaburagi).

REFERENCES

1. **Araki E, Lipes MA, Patti ME, Bruning JC, Haag B III, Johnson RS, and Kahn CR.** Alternative pathway of insulin signalling in mice with targeted disruption of the IRS-1 gene. *Nature* 372: 186–190, 1994.
2. **Blommaart EF, Luiken JJ, Blommaart PJ, van Woerkom GM, and Meijer AJ.** Phosphorylation of ribosomal protein S6 is inhibitory for autophagy in isolated rat hepatocytes. *J Biol Chem* 270: 2320–2326, 1995.
3. **Edvardsson U, Alexandersson M, Brockenhuus von Lowenhielm H., Nystrom AC, Ljung B, Nilsson F, and Dahllof B.** A proteome analysis of livers from obese (ob/ob) mice treated with the peroxisome proliferator WY14,643. *Electrophoresis* 20: 935–942, 1999.
4. **Fischer DC, Noack K, Runnebaum IB, Watermann DO, Kieback DG, Stamm S, and Stickeler E.** Expression of splicing factors in human ovarian cancer. *Oncol Rep* 11: 1085–1090, 2004.
5. **Harrop SJ, DeMaere MZ, Fairlie WD, Reztsova T, Valenzuela SM, Mazzanti M, Tonini R, Qiu MR, Jankova L, Warton K, Bauskin AR, Wu WM, Pankhurst S, Campbell TJ, Breit SN, and Curmi PM.** Crystal structure of a soluble form of the intracellular chloride ion channel CLIC1 (NCC27) at 1.4-A resolution. *J Biol Chem* 276: 44993–5000, 2001.
6. **Hatayama I, Yamada Y, Tanaka K, Ichihara A, and Sato K.** Induction of glutathione S-transferase P-form in primary cultured rat hepatocytes by epidermal growth factor and insulin. *Jpn J Cancer Res* 82: 807–814, 1991.
7. **Jaleel A and Nair KS.** Identification of multiple proteins whose synthetic rates are enhanced by high amino acid levels in rat hepatocytes. *Am J Physiol Endocrinol Metab* 286: E950–E957, 2004.
8. **Joshi RL, Lamothe B, Cordonnier N, Mesbah K, Monthioux E, Jami J, and Bucchini D.** Targeted disruption of the insulin receptor gene in the mouse results in neonatal lethality. *EMBO J* 15: 1542–1547, 1996.
9. **Jumaa H, Guenet JL, and Nielsen P.** Regulated expression and RNA processing of transcripts from the Srp20 splicing factor gene during the cell cycle. *Mol Cell Biol* 17: 3116–3124, 1997.
10. **Jumaa H and Nielsen PJ.** The splicing factor SRp20 modifies splicing of its own mRNA and ASF/SF2 antagonizes this regulation. *EMBO J* 16: 5077–5085, 1997.
11. **Jumaa H, Wei G, and Nielsen PJ.** Blastocyst formation is blocked in mouse embryos lacking the splicing factor SRp20. *Curr Biol* 9: 899–902, 1999.
12. **Kaburagi Y, Yamauchi T, Yamamoto-Honda R, Ueki K, Tobe K, Akanuma Y, Yazaki Y, and Kadowaki T.** The mechanism of insulin-induced signal transduction mediated by the insulin receptor substrate family. *Endocr J* 46, *Suppl*: S25–S34, 1999.
13. **King GL and Loeken MR.** Hyperglycemia-induced oxidative stress in diabetic complications. *Histochem Cell Biol* 122: 333–338, 2004.
14. **Liu JP, Baker J, Perkins AS, Robertson EJ, and Efstratiadis A.** Mice carrying null mutations of the genes encoding insulin-like growth factor I (Igf-1) and type 1 IGF receptor (Igf1r). *Cell* 75: 59–72, 1993.
15. **Robertson RP.** Chronic oxidative stress as a central mechanism for glucose toxicity in pancreatic islet beta cells in diabetes. *J Biol Chem* 279: 42351–42354, 2004.
16. **Saeki K, Hong Z, Nakatsu M, Yoshimori T, Kabeya Y, Yamamoto A, Kaburagi Y, and Yuo A.** Insulin-dependent signaling regulates azurophil granule-selective macroautophagy in human myeloblastic cells. *J Leukoc Biol* 74: 1108–1116, 2003.
17. **Sasaoka T and Kobayashi M.** The functional significance of Shc in insulin signaling as a substrate of the insulin receptor. *Endocr J* 47: 373–381, 2000.
18. **Schmitz HD.** Reversible nuclear translocation of glyceraldehyde-3-phosphate dehydrogenase upon serum depletion. *Eur J Cell Biol* 80: 419–427, 2001.
19. **Shisheva A, Buxton J, and Czech MP.** Differential intracellular localizations of GDP dissociation inhibitor isoforms. Insulin-dependent redistribution of GDP dissociation inhibitor-2 in 3T3-L1 adipocytes. *J Biol Chem* 269: 23865–32868, 1994.
20. **Sun XJ, Rothenberg P, Kahn CR, Backer JM, Araki E, Wilden PA, Cahill DA, Goldstein BJ, and White MF.** Structure of the insulin receptor substrate IRS-1 defines a unique signal transduction protein. *Nature* 352: 73–77, 1991.
21. **Sun XJ, Wang LM, Zhang Y, Yenush L, Myers MG Jr, Glasheen E, Lane WS, Pierce JH, and White MF.** Role of IRS-2 in insulin and cytokine signalling. *Nature* 377: 173–177, 1995.
22. **Tobe K, Tamemoto H, Yamauchi T, Aizawa S, Yazaki Y, and Kadowaki T.** Identification of a 190-kDa protein as a novel substrate for the insulin receptor kinase functionally similar to insulin receptor substrate-1. *J Biol Chem* 270: 5698–5701, 1995.
23. **Toda T, Sugimoto M, Omori A, Matsuzaki T, Furuichi Y, and Kimura N.** Proteomic analysis of Epstein-Barr virus-transformed human B-lymphoblastoid cell lines before and after immortalization. *Electrophoresis* 21: 1814–1822, 2000.
24. **Valentinis B, Romano G, Peruzzi F, Morrione A, Prisco M, Soddu S, Cristofanelli B, Sacchi A, and Baserga R.** Growth and differentiation signals by the insulin-like growth factor 1 receptor in hemopoietic cells are mediated through different pathways. *J Biol Chem* 274: 12423–12430, 1999.
25. **Valenzuela SM, Martin DK, Por SB, Robbins JM, Warton K, Bootcov MR, Schofield PR, Campbell TJ, and Breit SN.** Molecular cloning and expression of a chloride ion channel of cell nuclei. *J Biol Chem* 272: 12575–12582, 1997.
26. **Warton K, Tonini R, Fairlie WD, Matthews JM, Valenzuela SM, Qiu MR, Wu WM, Pankhurst S, Bauskin AR, Harrop SJ, Campbell TJ, Curmi PM, Breit SN, and Mazzanti M.** Recombinant CLIC1 (NCC27) assembles in lipid bilayers via a pH-dependent two-state process to form chloride ion channels with identical characteristics to those observed in Chinese hamster ovary cells expressing CLIC1. *J Biol Chem* 277: 26003–26011, 2002.

American Journal of Physiology – Endocrinology and Metabolism

Downloaded from ajpendo.physiology.org on August 25, 2005

Develop. Growth Differ. (2006) **48**, 177–188 doi: 10.1111/j.1440-169x.2006.00855.x

Peroxisome proliferator-activated receptor γ ligands stimulate myeloid differentiation and lipogenensis in human leukemia NB4 cells

Etsuko Yasugi,[1,*] Akiko Horiuchi,[3] Isao Uemura,[4] Emiko Okuma,[1] Masami Nakatsu,[1] Kumiko Saeki,[1] Yasushi Kamisaka,[6] Hiroyuki Kagechika,[5] Kazuki Yasuda[2] and Akira Yuo[1]

Departments of [1]Hematology and [2]Metabolic Disorder, Research Institute, International Medical Center of Japan, 1-21-1, Toyama, Shinjuku-ku, Tokyo 162-8655, [3]Division of Natural Sciences, International Christian University, 3-10-2, Osawa, Mitaka-shi, Tokyo 181-8585, [4]Department of Biological Science, Graduate School of Science, Tokyo Metropolitan University, 1-1, Minamiosawa, Hachioji, Tokyo 192-0397, [5]School of Biomedical Science, Tokyo Medical and Dental University, 2-3-10 Kanda-Surugadai, Chiyoda-ku, Tokyo 101-0062, and [6]Lipid Engineering Research Group, Research Institute of Biological Resources, National Institute of Advanced Industrial Science and Technology, Tsukuba, Ibaraki 305-8566, Japan

Peroxisome proliferator-activated receptor γ (PPARγ) plays a central role in adipocyte and macrophage differentiation. Pioglitazone (Actos, AD4833), an antidiabetic drug, and 15-deoxy-$\Delta^{12,14}$-prostaglandin J2 (PGJ2) have recently been identified as synthetic and natural ligands for PPARγ, respectively. In this study, we examined the effects of PPARγ ligands on differentiation and lipogenesis in promyelocytic leukemia NB4 cells, in which PPARγ protein was expressed and ligand-stimulated PPARγ-specific transcription of adipocyte fatty-acid binding protein was confirmed. Treatment with PPARγ ligand (AD4833 or PGJ2) alone markedly suppressed proliferation but did not induce differentiation. The combined treatment of the cells with PPARγ ligand and all-trans retinoic acid (ATRA) synergistically induced myelocytic differentiation, as determined by nitroblue tetrazolium reducing ability and cell morphology. During these processes of differentiation, we observed marked accumulation of lipid droplets in the cytoplasm. The cellular triacylglycerol levels increased 2.7-fold after treatment with the inducers. Simultaneously, BODIPY-fatty acid was incorporated into the cytosol and concentrated in lipid droplets. The biosynthesis of triacylglycerol-containing BODIPY-fatty acids was increased twofold in differentiated cells. These findings clearly demonstrate that treatment with PPARγ ligands not only induced differentiation but also stimulated lipogenesis in NB4 cells, indicating a close association between differentiation and lipogenesis in PPARγ-stimulated human myeloid cells.

Key words: differentiation, lipogenesis, NB4 cell, pioglitazone, PPARγ ligand.

Introduction

Peroxisome proliferator-activated receptor γ (PPARγ) is a member of the nuclear receptor superfamily and is a ligand-dependent transcription factor (Kliewer *et al.* 1992a; Kliewer *et al.* 1992b). This receptor functions as a central regulator in the process of adipocyte or macrophage differentiation as well as in lipid and glucose metabolism (Nagy *et al.* 1998; Tontonoz *et al.* 1998; Rosen *et al.* 1999). Its ligands include modified fatty acids, the prostaglandin D2 metabolite 15-deoxy-$\Delta^{12,14}$-prostaglandin J2 (PGJ2), and antidiabetic drugs such as thiazolidione, rosiglitazone or pioglitazone (Forman *et al.* 1995; Lehmann *et al.* 1995; Nagy *et al.* 1998). PPARγ binds to DNA as a heterodimer with the retinoid X receptor (RXR). This heterodimer is also activated by RXR ligands (Kliewer *et al.* 1992b; Gearing *et al.* 1993). Together, ligands specific for PPARγ and RXR can synergistically activate transcription and promote adipocyte differentiation in culture (Schulman *et al.* 1998; Thuillier *et al.* 1998).

In several myelocytic cell lines, such as HL-60, U937 and NB4, all-trans retinoic acid (ATRA), which binds to retinoic acid receptors (RAR), induces differentiation of these immature myeloid cells into mature phagocytic cells (Breitman *et al.* 1980; Hu *et al.* 1993). ATRA has

Etsuko Yasugi and Akiko Horiuchi contributed equally to this work.
*Author to whom all correspondence should be addressed.
Email: e-yasugi@umin.ac.jp
Received 5 December 2005; revised 18 January 2006; accepted 19 January 2006.

been used successfully for the treatment of patients with acute promyelocytic leukemia (APL; Huang *et al.* 1988; Degos 1992). However, this therapy has one problem, that is, the prolonged use of a high dose of ATRA provoked expression of cytosolic retinoic acid-binding proteins, which resulted in the leukemic cells becoming resistant to the induction of differentiation (Cornic *et al.* 1992). 9-*cis*-Retinoic acid (9-*cis* RA), an isomer of ATRA that can bind both RAR and RXR, also proved to be potent in inducing differentiation (Kizaki *et al.* 1993; Sakashita *et al.* 1993). In addition, Evans *et al.* reported that the combination of a PPARγ ligand and an RXRα ligand induced monocytic differentiation of some myeloid leukemia cell lines (HL-60 and THP-1) (Nagy *et al.* 1998; Tontonoz *et al.* 1998). Therefore, we considered that the combination of PPARγ ligands with retinoids, not only RXR ligands but also RAR ligands, might have synergetic effects on differentiation in the APL cell line NB4.

Peroxisome proliferator-activated receptor γ functions as a transcriptional regulator of genes related to lipid metabolism. Known targets of PPARγ include the genes encoding adipocyte fatty acid binding protein (aP2), phosphoenoylpyruvate carboxykinase, lipoprotein lipase, and the brown fat uncoupling protein UCP1 (Tontonoz *et al.* 1998). PPARγ is expressed at high levels in adipose tissues and serves as a central regulator of the process of adipocyte differentiation (Chawla *et al.* 1994; Tontonoz *et al.* 1994). This transcription factor may also play an important role in the regulation of lipid metabolism in other cell types, such as cells in mammary and colonic epithelia (Mueller *et al.* 1998) and monocyte/macrophages (Tontonoz *et al.* 1998). These facts led us to study the effects of PPARγ ligands in combination with a retinoid on lipogenesis in human myeloid NB4 cells.

In this study, we investigated the combined effects of ATRA (RAR ligand) and PPARγ ligands on human myeloid NB4 cells. Two major cell biological phenomena on which we focused were differentiation and lipogenesis, since RAR and PPARγ play important roles in both of these biological phenomena in human myeloid cells, and therefore we can explore possible linkage between them in our *in vitro* assay system. Our data showed that pioglitazone or PGJ2 in conjunction with ATRA inhibited clonal proliferation and potently induced the differentiation of NB4 cells to granulocytic maturation. Furthermore, cells exposed to the combination of PPARγ ligand and ATRA accumulated lipid droplets. The levels and biosynthesis of triacylglycerol in the cells increased markedly after differentiation. Taken together, these findings show that treatment with PPARγ ligand and ATRA exerted synergistic effects on differentiation and lipogenesis in NB4 cells.

Materials and methods

Chemicals

All-trans retinoic acid, PGJ2, and the synthetic PPARγ ligand pioglitazone (Actos, AD4833) were obtained from Sigma-Aldrich (St Louis, MO, USA), Cayman Chemical (Ann Arbor, MI, USA) and Takeda Chemical Industries, (Tokyo, Japan), respectively. These reagents were dissolved in ethanol. PPARγ antagonist (GW9662), RXR antagonist (HX531) and RXR agonists (LG100268, PA024) were synthesized (Boehm *et al.* 1995; Ebisawa *et al.* 1999; Ohta *et al.* 2000; Willson *et al.* 2001). PPARγ antagonist (BADGE) was obtained from Cayman Chemicals. All antagonists and agonists were dissolved in ethanol. Diluent alone had no effect on the proliferation or differentiation of leukemia cell lines. BODIPY FL dodecanoic acid (BODIPY-FL-C12), cholesteryl BODIPY FL C12 and nile red were from Molecular Probes (Eugene, OR, USA). Triacylglycerol-containing BODIPY-FL-C12 was synthesized from 1, 2-diacylglyceride (Funakoshi Co., Tokyo, Japan) and BODIPY-FL-C12 using Lipase D derived from Rhizopus delemar (Amano Pharmaceutical Co., Nagoya, Japan). Anti-PPARγ (H-100) antibody was obtained from Santa-Cruz Biotechnology (Santa Cruz, CA, USA).

Cell culture

Human myelocytic leukemia cell lines (NB4 and HL-60) were grown in RPMI-1640 medium (Sigma-Ardrich) with 10% fetal calf serum (FCS; JRH Biosciences, Lenexa, KS, USA) at 37°C in an atmosphere of 5% CO_2. Cell suspension (4×10^4 cells/mL) in RPMI-1640 medium containing 10% FCS was placed in each well of 6-well plates or 24-well plates. PPARγ ligand and ATRA were added to the culture medium. The cells were incubated for the indicated periods and harvested for experiments. To examine the effect of antagonists, the cells were pretreated with antagonist for 8 h prior to treatment.

Assessment of cell proliferation and differentiation

Cell growth after various treatments was assessed by counting viable cells under a phase contrast microscope (Olympus CK40; Olympus, Tokyo, Japan). Differentiation of leukemia cells was examined by assessing their ability to produce superoxide, as measured by reduction of nitroblue tetrazolium (NBT; Nacarai Tesque, Kyoto, Japan). For analysis of the ability to reduce NBT, samples of cultured cells were washed once and then suspended in RPMI-1640 medium supplemented with 10% FCS containing 1 mg/mL NBT and 100 ng/mL 12-O-tetradecanoylphorbol 13-acetate (Sigma) for 30 min at 37°C. Cells containing

formazan blue-black deposits were detected light microscopy (Olympus BX-51) and counted. To further confirm cell differentiation, cytocentrifuged preparations of cells were stained with Wright-Giemsa solution and observed under a light microscope.

Ultrastructural analysis

For morphological observation of differentiation and lipid droplets, electron microscopy was used. Methods of fixation, staining, embedding and sectioning were described previously (Yasugi *et al.* 2002). Sections were examined with an electron microscope (JEOL JEM1010; JEOL, Tokyo, Japan) and images were taken with the Imaging Plate system (PIX system 20; JEOL).

Preparation of cell lysates, gel electrophoresis and immunoblotting

Cell pellets were suspended in 1× sample buffer and mixed vigorously. The cell suspension was heated for 5 min at 100°C and then frozen at –20°C until use. Proteins were separated by electrophoresis in a 10% sodium dodecyl sulfate–polyacrylamide gel and transferred to a polyvinylidene difluoride membrane in blotting buffer. After transfer, the membrane was blocked with 5% non-fat dry milk in phosphate-buffered saline (PBS) for 1 h at room temperature. After incubation with primary antibody against PPARγ, horseradish peroxidase-conjugated secondary antibody followed by the enhanced chemiluminescence (ECL) system from Amersham Biosciences (Piscataway, NJ, USA) were used for detection.

RNA analysis

Total RNA was obtained from cells using an RNeasy mini kit (QIAGEN, Hilden, Germany). The first strand cDNA was synthesized from 1 μg of total RNA using the Super Script II Transcriptase (Invitrogen Japan, Tokyo, Japan). For the polymerase chain reaction (PCR) assay, 1 μL of cDNA was used in a total volume of 50 μL containing 1× reaction buffer, 0.2 mM dNTP, 20 pmol of each primer, and 0.25 U of Ex Taq polymerase (Takara Bio., Otsu, Japan). PCR was performed in a GeneAmp PCR system 9600 (Applied Biosystems, Foster City, CA, USA) with the following temperature profile: denaturation at 95°C, primer annealing at 55°C, and primer extension at 72°C, each for 30 s. After an initial denaturation (95°C, 5 min), the cycle was performed 30 times, followed by a final extension step for 7 min at 72°C. The primers used for aP2 (Genbank accession number J02874) were as follows: sense primer, 5′-TCCAGTGAAAACTTTGATGATTAT-3′; antisense primer, 5′-ACGCATTCCACCACCAGTTTA-3′); as described before (Zilberfarb *et al.* 2001). The expected size of the PCR product was 320 bp. PCR products were visualized on a 2% agarose gel by ethidium bromide staining.

Lipid droplet staining in cells

Cells were fixed with 1% paraformaldehyde in PBS for 30 min at room temperature and washed with PBS. For detection of lipid droplets, the cells were stained with nile red at a final concentration of 0.1 μg/mL for 30 min at room temperature, and examined with a fluorescence microscope (Olympus BX-51). The cell morphology in the same fluorescent image was observed under a light microscope with Nomarski differential interference contrast (DIC). The fluorescent and DIC images of cells were captured by Aquacosmos (version 2.01) from a digital camera C4742-95 (Hamamatsu Photonics, Hamamatsu, Japan).

Quantitation of triacylglycerol

Each sample of cells was harvested after 4 days of treatment with PPARγ ligand and ATRA, and sonicated in water. Lipids were extracted from the homogenate with methanol–chloroform–water (2:1:0.8, v/v). Extracted lipid was evaporated to dryness and dissolved in chloroform–methanol (2:1, v/v). Total lipid was applied to a high performance thin-layer chromatography (HPTLC) silica gel plate (Kieselgel 60; Merk & Co., Whitehouse Station, NJ, USA). For detection of neutral lipid, the plate was developed with a solvent mixture of hexane–ethylacetate (1:1, v/v) and was stained with Morstein reagent (10% sulfuric acid solution containing 0.1% cesium sulfate and 5% ammonium pentamolybdate). Levels of triacylglycerol in cells were quantified enzymatically using a Triglyceride *G*-test Wako kit (Wako Pure Chemical Industries, Osaka, Japan).

Metabolism of fluorescent fatty acid analogues in NB4 cells

After treatment with PPARγ ligand and ATRA for 3 days, cells in 96-well plates were incubated in RPMI medium containing BODIPY-FL-C12 (10 ng/mL) for 2 min at room temperature. After washing, cells were subsequently chased in RPMI medium at room temperature for various periods and examined using a fluorescence microscope. The intensity of incorporated BODIPY-FL-C12 fluorescence in the cells was analyzed using a FluorImager 595 (Amersham Biosciences).

For detection of triacylglycerol synthesis, cells were incubated with BODIPY-FL-C12 for 10 min at room temperature, washed and further incubated for

30 min at 37°C. Lipids extracted from the cells were separated on HPTLC plates with a solvent mixture of hexane–diethylether (1:1, v/v), visualized using a FluorImager 595, and quantified as percentage using Image Quant software.

Triacylglycerol synthesis was assayed *in vitro* in a final volume of 300 μL containing 16 μM BODIPY-FL-C12, 36 μM coenzyme A sodium salt, 0.5 M Tris-HCl buffer (pH 7.5) and cell homogenate (125 μg of protein) as an enzyme source. Glycerol and dihydroxyacetone phosphate lithium salt were used as substrates. Incubation was carried out for 30 min at room temperature and terminated by the addition of 2 mL of ethyl acetate. Lipids were extracted twice with ethyl acetate for 2 min by vigorously shaking. Then the combined organic phases were applied to HPTLC plates. Triacylglycerol containing BODIPY-FL-C12 was visualized with a FluorImager 595 and its amount was estimated as described above.

Protein determination

Protein content was measured using the BCA Protein Assay Reagent (Pierce, Rockford, IL, USA).

Statistical analysis

Statistical significance was determined by using Student's *t*-test (two-tailed) to compare the two groups of data sets. Asterisks shown in the figures and tables indicate significant differences between experimental conditions and the corresponding control condition.

Results

Presence of peroxisome proliferator-activated receptor γ protein and the growth-suppressive effect of peroxisome proliferator-activated receptor γ ligands in myeloid cells

Peroxisome proliferator-activated receptor γ protein in untreated and differentiated NB4 cells was detected by western blotting. The relative molecular mass of the PPARγ protein was 52 KDa. The expression of PPARγ protein was found in untreated cells. Treatment with PPARγ ligand alone or with a combination of PPARγ ligand and ATRA for 2 days (Fig. 1) or 4 days (data not shown) resulted in expression levels equivalent to those in untreated cells.

The effects of PPARγ ligand and ATRA on the proliferation of NB4 cells are shown in Table 1. PPARγ ligand (PGJ2 (4 μM) or AD4833 (50 μM)) alone caused a dramatic decrease of cell growth after 4 days of incubation, though ATRA (1 nM) had less effect. Combined treatment with ATRA plus PGJ2 or AD4833 caused a further decrease in the number of viable cells.

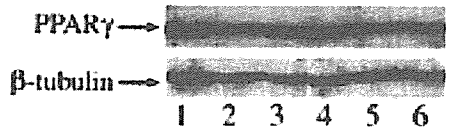

Fig. 1. Intracellular levels of peroxisome proliferator-activated receptor γ (PPARγ) protein in NB4 cells. Cells were treated with PPARγ ligand and/or all-trans retinoic acid (ATRA) for 2 days, and then whole cell extracts were subjected to western blot analysis. 1, Control; 2, 1 μM ATRA; 3, 4 μM 15-deoxy-Δ12,14-prostaglandin J2 (PGJ2); 4, 50 μM AD4833; 5, 1 μM ATRA + 4 μM PGJ2; 6, 1 μM ATRA + 50 μM AD4833.

Table 1. Effects of peroxisome proliferator-activated receptor γ ligands on NB4 cell growth

Treatment	Cell number ($\times 10^4$)
Untreated	106.0 ± 4.3
1 nM ATRA	79.5 ± 3.5
4 μM PGJ2	34.7 ± 2.6
50 μM AD4833	47.0 ± 5.2
1 nμ ATRA + 4 μM PGJ2	26.7 ± 0.9
1 nM ATRA + 50 μM AD4833	31.7 ± 3.3

Cell number was counted after 4 days of treatment. Values are mean ± SD. ATRA, all-trans retinoic acid; PGJ2, 15-deoxy-Δ12,14-prostaglandin J2.

Peroxisome proliferator-activated receptor γ ligand and all-trans retinoic acid cooperate to promote NB4 differentiation

The differentiation of NB4 cells was evaluated by assessing the ability to reduce NBT, Wright-Giemsa staining and electron microscopic observation. With regard to NBT-reducing activity, neither PGJ2 nor AD4833 alone increased the activity of cells (data not shown). The combined treatment of cells with ATRA (1 nM) and PPARγ ligand strongly enhanced the NBT-reducing activity. More than 90% of cells treated with PPARγ ligand plus ATRA cells were positive for this activity, although ATRA-treated cells showed only 22% positivity (Fig. 2a). A high concentration of ATRA (1 μM) alone resulted in 96% of the cells being positive for NBT-reducing activity. In HL-60 cells, similar effects of PPARγ ligands and ATRA on differentiation were observed, although treatment with PGJ2 or AD4833 alone induced differentiation in these cells (Fig. 2b).

Next, the granulocytic differentiation of NB4 cells was morphologically confirmed by Wright-Giemsa staining (Fig. 3A). The cells treated with ATRA (1 nM) and PPARγ ligand showed lobulated kidney-bean or

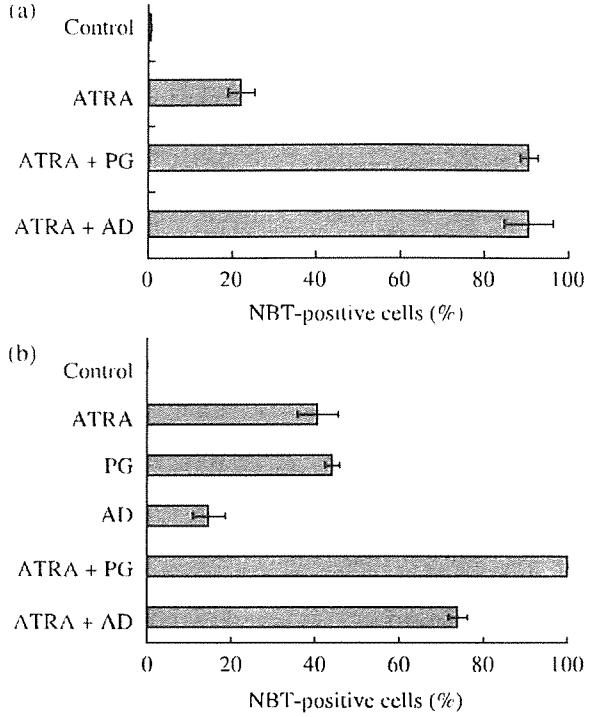

Fig. 2. Effects of peroxisome proliferator-activated receptor γ (PPARγ) ligands on nitroblue tetrazolium (NBT)-reducing activity in human myeloid cells. The NBT-reducing activities of NB4 (a) and HL-60 cells (b) were determined after 4 days of treatment with the indicated reagents. The activities are expressed as the percentage of NBT-positive cells. Results are representative of three experiments and are expressed as mean ± SD. (a) ATRA, 1 nM all-trans retinoic acid (ATRA); PG, 4 μM 15-deoxy-Δ12,14-prostaglandin J2 (PGJ2); AD, 50 μM AD4833. (b) ATRA, 1 μM ATRA; PG, 4 μM PGJ2; AD, 50 μM AD4833.

horse-shoe-shaped nuclei that are characteristic of granulocytes. The cytoplasm of those cells contained many white vacuoles and was stained white, in contrast to the blue cytoplasm of control cells. Furthermore ultrastructural observation showed that the combined treatment of cells with PPARγ ligand and ATRA (1 nM) induced irregularly lobulated nuclei and condensation of heterochromatin along the nuclear membrane (Fig. 3B). These results clearly indicate that PPARγ ligand and ATRA showed synergistic effects on granulocytic differentiation of NB4 cells.

Effects of peroxisome proliferator-activated receptor γ and retinoid X receptor antagonists on differentiation of NB4 cells

To confirm that the differentiation of NB4 cells is mediated through the PPARγ pathway, we used antagonists of PPARγ and RXR, such as GW9662 (Willson *et al.* 2001), BADGE (Wright *et al.* 2000) and HX531. HX531 works as an RXR antagonist (Ebisawa *et al.* 1999) but also as a potential PPARγ/RXR inhibitor (Yamauchi *et al.* 2001). The effects of PPARγ and RXR antagonists were evaluated in terms of the induced-differentiation of NB4 cells as determined by the NBT reduction assay. Their effects on ATRA ligand- and PPARγ ligand-induced NB4 differentiation are summarized in Table 2. All three antagonists showed inhibitory effects on the differentiation induced by the combination of ATRA and PPARγ ligands. In contrast, PPARγ antagonists did not exert an inhibitory effect on the differentiation of NB4 cells induced by ATRA

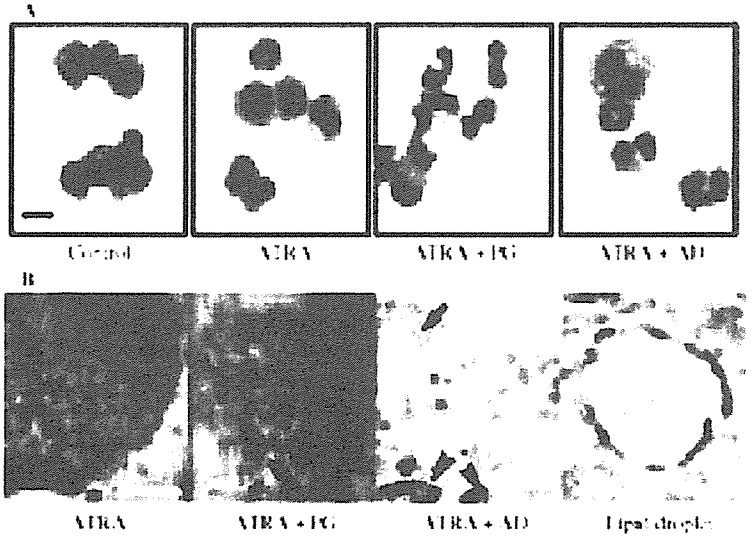

Fig. 3. Morphological observation of NB4 cells treated with peroxisome proliferator-activated receptor γ (PPARγ) ligand and/or all-trans retinoic acid (ATRA). The cells were treated for 4 days with ATRA (1 nM), PG (4 μM 15-deoxy-Δ12,14-prostaglandin J2), AD (50 μM AD4833), individually or combined. (A) Wright-Giemsa staining. Bar, 20 μm (B) Ultrastructural observation. Arrowhead and arrow indicate nucleus and lipid droplet, respectively. Bar, 4 μm. Right panel is higher magnification of the lipid droplet. Bar, 0.5 μm.

Table 2. Effects of peroxisome proliferator-activated receptor γ antagonists on NB4 differentiation

	None	HX531	GW9662	BADGE
1 μM ATRA	96.1 ± 2.2	95.0 ± 2.0	97.1 ± 0.2	94.3 ± 2.1
1 nM ATRA	22.0 ± 3.2	12.0 ± 2.2*	16.5 ± 8.8	25.5 ± 3.4
1 nM ATRA + 0.5 μM PGJ2	39.4 ± 4.9			28.7 ± 3.3*
1 nM ATRA + 2 μM PGJ2	91.7 ± 4.7	15.3 ± 1.0**	19.2 ± 3.8**	92.2 ± 2.1
1 nM ATRA + 50 μM AD4833	90.4 ± 5.8	3.2 ± 0.6***	5.6 ± 0.8***	26.3 ± 6.9**

Concentration of each antagonist was 1 μM. Values are expressed as percent of NBT-positive cells. Values are mean ± SD. Probabilities were calculated for the percentages of NBT-positive cells with and without peroxisome proliferator-activated receptor γ antagonist. *$P < 0.05$, **$P < 0.01$, ***$P < 0.001$. ATRA, all-trans retinoic acid; PGJ2, 15-deoxy-Δ ^{12,14}-prostaglandin J2.

Table 3. Effects of retinoic X receptor agonists on NB4 differentiation

	LG100268	PA024
None	0.8 ± 0.1	2.9 ± 0.7
4 μM PGJ2	74.8 ± 7.4***	26.3 ± 5.4**
50 μM AD4833	17.0 ± 1.3**	13.3 ± 3.5*

Concentration of each agonist was 1 μM. Values are expressed as percent of NBT-positive cells. Values are mean ± SD. Probabilities were calculated for the percentages of NBT-positive cells with and without peroxisome proliferator-activated receptor γ ligand. *$P < 0.05$, **$P < 0.01$, ***$P < 0.005$. PGJ2, 15-deoxy-Δ ^{12,14}-prostaglandin J2.

(1 nM or 1 μM) alone. Thus, for the induction of differentiation by the combination of ATRA and PPARγ ligands, the signaling through PPARγ/RXR is necessary. The combination of RXR agonist and PPARγ ligand also induced NB4 differentiation, indicating that the stimulation of the RXR receptor is important in this differentiation pathway (Table 3).

Upregulation of adipocyte fatty acid binding protein in NB4 cells during treatment with peroxisome proliferator-activated receptor γ ligands

The expression of adipocyte fatty acid binding protein (aP2), whose promoter has an adipose response element (ARE; DR-1), occurs in parallel to the expression of PPARγ (Thuillier *et al.* 1998). We examined the gene expression of aP2 in NB4 cells by reverse transcription–polymerase chain reaction (RT–PCR) after treatment with ATRA (1 μM) and PPARγ ligand (Fig. 4). The expression of aP2 mRNA was greatly induced after 24 h and continued for up to 4 days in NB4 cells cultured with PPARγ ligand alone or with a combination of PPARγ ligand and ATRA, whereas the expression of this gene remained low or undetectable in cells cultured with ATRA alone or in untreated cells. Thus, in human myeloid cells, PPARγ ligands induced the transcription of a gene

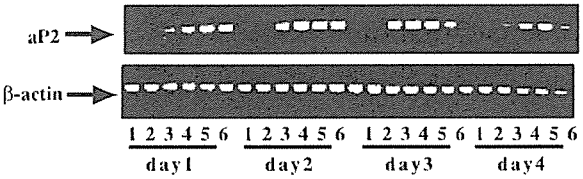

Fig. 4. Adipocyte fatty acid binding protein (aP2) mRNA expression in NB4 cells after treatment with peroxisome proliferator-activated receptor γ (PPARγ) ligand and/or all-trans retinoic acid (ATRA). Cells were treated with PPARγ ligand and/or ATRA for the indicated periods. Reverse transcription–polymerase chain reaction for aP2 mRNA in freshly prepared NB4 cells revealed a cDNA fragment of the expected size. 1, Control; 2, 1 μM ATRA; 3, 1 μM ATRA + 4 μM PGJ2; 4, 1 μM ATRA + 50 μM AD4833; 5, 4 μM PGJ2; 6, 50 μM AD4833. As a control for cDNA quality, the signals for β-actin expression are shown.

specific for this transcriptional receptor and important for lipid metabolism.

Lipid droplets accumulate in NB4 cells after treatment with peroxisome proliferator-activated receptor γ ligands and all-trans retinoic acid

In the cytoplasm of cells treated with PPARγ ligands and ATRA, we found many white vacuoles after Wright-Giemsa-staining, as mentioned above (Fig. 3A). We speculated that these vacuoles might be lipid droplets and examined the cells by fluorescence microscopy after staining with the lipophilic dye nile red. As nile red has the remarkable property of staining neutral lipids (Greenspan *et al.* 1985), lipid droplets containing triacylglycerol or cholesterol ester show a fluorescent red color. In Figure 5A, NB4 cells after treatment with PPARγ ligands and ATRA (1 μM) contained numerous nile red-positive droplets. In the cytoplasm of cells treated with ATRA alone, there were also lipid droplets, but the number of droplets was fewer and the intensity of the fluorescence was weaker. In the cells treated with PGJ2 or AD4833 alone, lipid droplets were weakly visible (data not

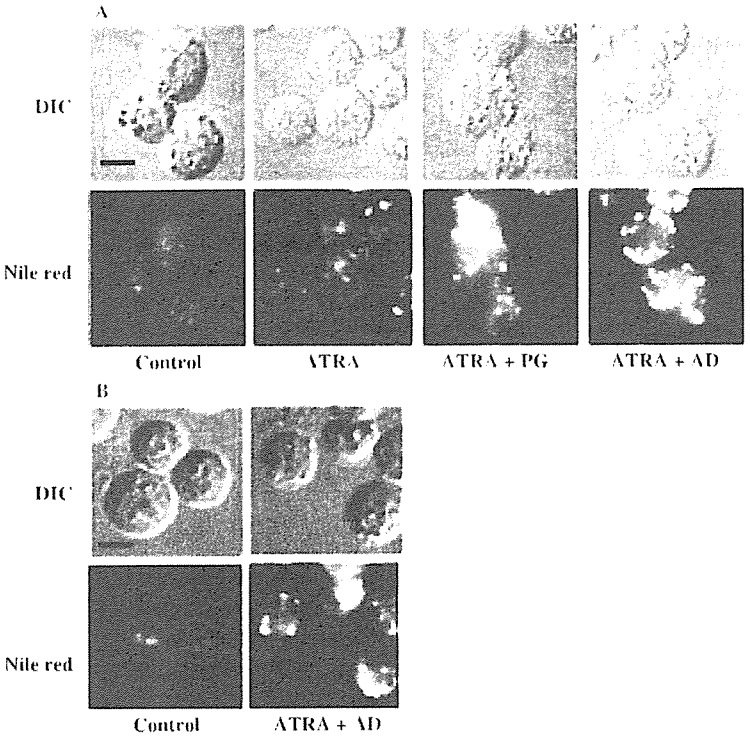

Fig. 5. Accumulation of lipid droplets in differentiated NB4 and HL-60 cells. Cells were treated for 4 days with all-trans retinoic acid (ATRA; 1 μM), ATRA (1 μM) + 15-deoxy-Δ12,14-prostaglandin J2 (PG; 4 μM) or ATRA (1 μM) + AD4833 (AD; 50 μM). Upper panels are difference interference contrast images, and lower panels are the corresponding images obtained by fluorescence microscopy. Lipid droplets were stained with nile red. Bar, 10 μm. (A) NB4 cells, (B) HL-60 cells.

shown). Similar findings were made in HL-60 cells (Fig. 5B). Ultrastructural observation revealed that treatment with PPARγ ligand and ATRA clearly stimulated the accumulation of lipid droplets in the cytoplasm (Fig. 3B). Lipid droplets are surrounded by a phospholipid monolayer, and clearly distinguished from other organelles in the cytoplasm. Both types of microscopic observation clearly demonstrated that PPARγ ligands stimulated the accumulation of lipid droplets in NB4 cells.

Triacylglycerol levels increase in NB4 cells after treatment with peroxisome proliferator-activated receptor γ ligands and all-trans retinoic acid

We examined whether treatment with PPARγ ligand and ATRA (1 μM) affected the cellular levels of triacylglycerol and cholesterol ester, the major storage lipids in mammalian cells. Thin-layer chromatography revealed that treatment with PPARγ ligand and ATRA particularly increased the triacylglycerol level in NB4 cells, and slightly increased the cholesterol ester level (Fig. 6a). Free-cholesterol levels were almost equivalent between untreated cells and cells treated with PPARγ ligand and ATRA. Next, the cellular triacylglycerol levels were analyzed enzymatically (Fig. 6b). After incubation with ATRA (1 μM) combined with PGJ2 or AD4833, the triacylglycerol level of NB4 cells was increased by 2.7-fold compared to that in untreated cells. PGJ2 or AD4833 alone also increased the triacylglycerol level slightly, but ATRA alone did not. These results strongly suggest that the lipid droplets in NB4 cells contained predominantly triacylglycerol, and the level of triacylglycerol increased after treatment of the cells with PPARγ ligand and ATRA.

Translocation of a fluorescent fatty acid analogue, BODIPY-FL-C12 in NB4 cells treated with peroxisome proliferator-activated receptor γ ligands and all-trans retinoic acid

The distribution pattern of intracellular BODIPY fluorescence was compared between differentiated and untreated cells under the pulse-chase conditions (Fig. 7a). After prelabeling of cells with BODIPY-FL-C12 at room temperature, intracellular fluorescence was distributed in the cytoplasm, including the endoplasmic reticulum (ER), in both differentiated and untreated cells. After a chase of 10–30 min, most of the intracellular fluorescence in differentiated cells was clearly accumulated in the lipid droplets, though that in untreated cells remained in the cytoplasm. The translocation of the fluorescence from the cytosol to lipid droplets was observed in differentiated cells treated with ATRA alone or with ATRA and PPARγ ligand. There was no significant difference in total

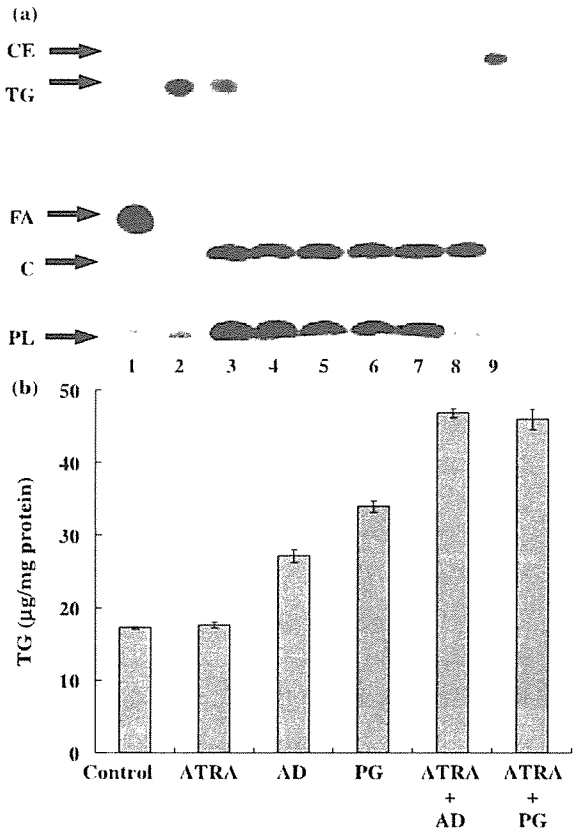

Fig. 6. (a) Thin-layer chromatogram of neutral lipids in differentiated NB4 cells. Each lane was spotted with crude lipid extracted from 7×10^4 cells. Cells were treated for 4 days with peroxisome proliferator-activated receptor γ (PPARγ) ligands and/or all-trans retinoic acid (ATRA). 1, linoleic acid; 2, trilinolein; 3, 1 μM ATRA + 4 μM 15-deoxy-Δ12,14-prostaglandin J2 (PGJ2); 4, control; 5, 1 μM ATRA + 50 μM AD4833; 6, 1 μM ATRA; 7, control; 8, cholesterol; 9, cholesterol ester. CE, cholesterol ester; TG, triacylglycerol; FA, fatty acid; C, cholesterol; PL, phospholipid. (b) Triacylglycerol levels in differentiated NB4 cells. Cells were treated for 4 days with PPARγ ligand and/or ATRA (1 μM). PG, 4 μM PGJ2; AD, 50 μM AD4833. Values represent mean ± SD. Triacylglycerol contents are expressed as μg/mg protein.

amount of BODIPY lipid associated with cells between the differentiated and untreated cells (data not shown). These observations provided evidence that BODIPY-FL-C12 was incorporated in the cytoplasm and immediately translocated to lipid droplets in differentiated cells.

Metabolism of BODIPY-FL-C12 in NB4 cells treated with peroxisome proliferator-activated receptor γ ligands and all-trans retinoic acid

In order to examine the metabolism of incorporated BODIPY-FL-C12, cells were prelabeled with BODIPY-FL-C12 at room temperature for 10 min and incubated for 30 min at 37°C. Extracted lipids containing BODIPY-FL-C12 were analyzed by thin-layer chromatography using a FluorImager. The fluorescent spots of triacylglycerol containing BODIPY-FL-C12 were detected in lipids extracted from both differentiated and untreated cells (data not shown). The Rf value of triacylglycerol containing BODIPY-FL-C12 was confirmed by the comigration of synthesized triacylglycerol containing BODIPY-FL-C12. The fluorescence of triacylglycerol extracted from cells treated with PPARγ ligands and ATRA was about twofold stronger than that of untreated cells (Fig. 7b). These findings indicated that BODIPY-FL-C12 had been incorporated in the cytoplasm and converted to triacylglycerol.

Triacylglycerol synthesis activity in differentiated and untreated cell homogenates was compared using two substrates, glycerol and dihydroxyacetone phosphate, respectively. The activity in differentiated cells treated with PPARγ ligands and ATRA was found to be more than twofold higher than that in untreated cells using glycerol as substrate (Fig. 7c). The activity was dependent on glycerol concentration (Fig. 7c) but not on dihydroxyacetone phosphate (data not shown).

These findings suggest that triacylglycerol was synthesized from glycerol in differentiated cells. Taken together, these data show that triacylglycerol synthesis in NB4 cells treated with PPARγ ligand and ATRA increased.

Discussion

Peroxisome proliferator-activated receptor γ has been demonstrated to regulate adipocyte differentiation and glucose homeostasis in response to several structurally distinct compounds, including thiazolidinediones (Tontonoz *et al.* 1994; Lehmann *et al.* 1995). In this study, we investigated the effects of PPARγ ligands on human NB4 and HL-60 cells and found that PPARγ ligands can act synergistically with ATRA to induce differentiation into cells that show granulocytic characteristics and accumulate lipid droplets. Activation of PPARγ in immortalized cell lines, such as THP-1 and HL-60, promotes differentiation along the macrophage lineage, as shown by changes in gene expression and uptake of OxLDL induced by CD36 (Hirase *et al.* 1999; Tontonoz *et al.* 1998). However, using PPARγ -deficient stem cells, Moore *et al.* demonstrated that PPARγ is neither essential for myeloid development nor for mature macrophage functions such as phagocytosis and inflammatory production (Moore *et al.* 2001). Furthermore, Asou *et al.* reported the effects of troglitazone on the proliferation and

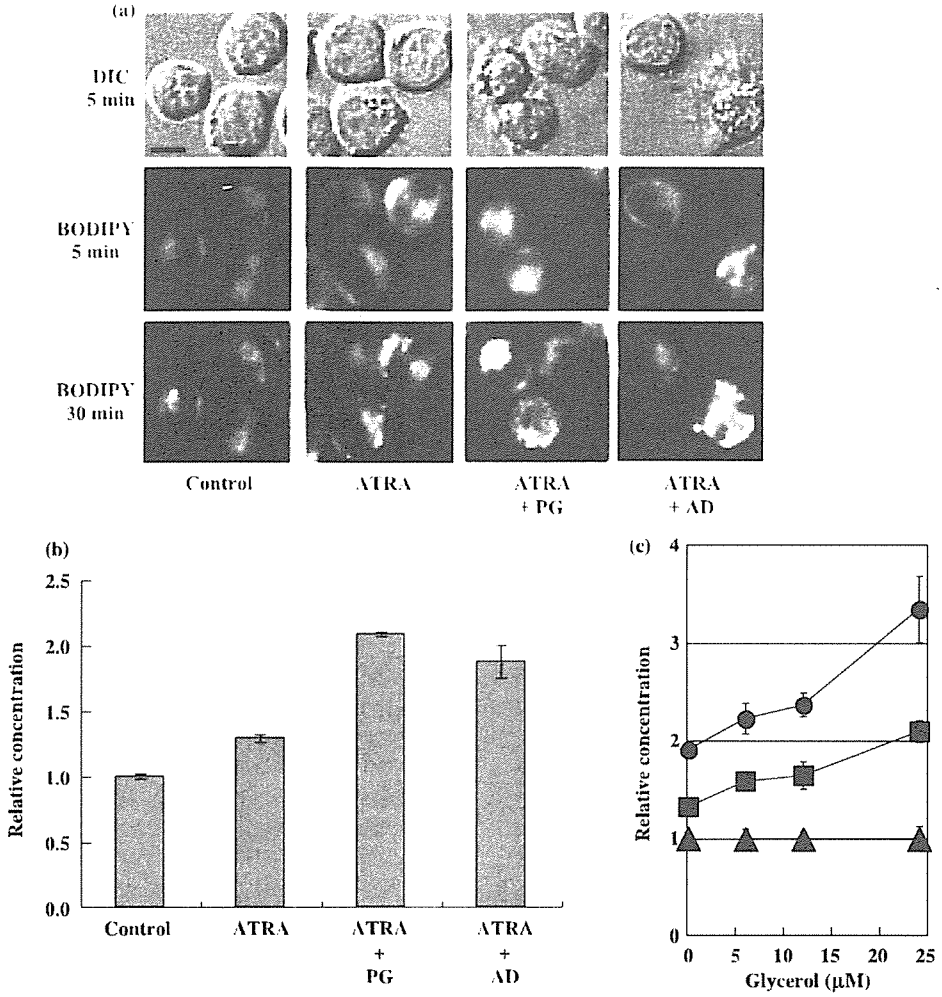

Fig. 7. (a) Intracellular distribution of BODIPY-FL-C12 fluorescence in differentiated and untreated NB4 cells. Cells were treated for 3 days with all-trans retinoic acid (ATRA; 1 μM), ATRA (1 μM) + 15-deoxy-Δ12,14-prostaglandin J2 (PG; 4 μM) or ATRA (1 μM) + AD (AD4833, 50 μM). Cells were incubated in medium containing BODIPY-FL-C12 for 2 min at room temperature and were subsequently chased and examined using a fluorescence microscope. Upper panels are difference interference contrast images. Middle and lower panels are the corresponding fluorescence microscopy images. BODIPY, BODIPY-FL-C12. Bar, 10 μm. (b) Relative concentration of triacylglycerol containing BODIPY-FL-C12 in NB4 cells. Cells were treated for 3 days with peroxisome proliferator-activated receptor γ (PPARγ) ligand (PGJ2 4 μM, AD4833 50 μM) and/or ATRA (1 μM). The assay methods are described in Materials and methods. Values represent mean ± SD. The relative concentrations of triacylglycerol containing BODIPY-FL-C12 in differentiated cells were calculated as fluorescence strength compared to that in untreated cells taken as 1.00. (c) Triacylglycerol synthesis activity in NB4 cells. Cells were treated for 3 days with PPARγ ligand (PGJ2 4 μM, AD4833 50 μM) and ATRA (1 μM). The method of the enzyme assay is described in Materials and methods. Values are mean ± SD. The relative concentrations of triacylglycerol containing BODIPY-FL-C12 in differentiated cells are plotted together with that of untreated cells taken as 1.00. (●), ATRA + PG; (■), ATRA + AD; (▲), control.

differentiation of normal and malignant myeloid cells (especially monocytic cells) and demonstrated that troglitazone combined with a retinoid was a moderately potent inhibitor of the clonogenic growth of acute myeloid leukemia cells, but not a potent inducer of differentiation of these leukemia cells (Asou *et al.* 1999). Our results clearly indicated that combined treatment with PPARγ ligand and ATRA induced differentiation of NB4 cells. This discrepancy between these findings may be related to the fact that in the study of Asou *et al.* (1999), NB4 cells were treated with troglitazone (10^{-5} M) as the PPARγ ligand, and the concentration of troglitazone was rather low compared to our conditions. We also examined the effects of PPARγ ligands and ATRA on HL-60 cells and observed synergistic effects of PPARγ ligands